21887

National Library of Canada / Bibliothèque nationale du Canada

CANADIAN THESES ON MICROFICHE / THÈSES CANADIENNES SUR MICROFICHE

NAME OF AUTHOR/*NOM DE L'AUTEUR* J. D. MCFARLAND

TITLE OF THESIS/*TITRE DE LA THÈSE* TRANSITION TO TURBULENCE IN FREE MIXING

UNIVERSITY/*UNIVERSITÉ* THE UNIVERSITY OF ALBERTA

DEGREE FOR WHICH THESIS WAS PRESENTED/*GRADE POUR LEQUEL CETTE THÈSE FUT PRÉSENTÉE* MASTER OF SCIENCE

YEAR THIS DEGREE CONFERRED/*ANNÉE D'OBTENTION DE CE DEGRÉ* 1974

NAME OF SUPERVISOR/*NOM DU DIRECTEUR DE THÈSE* P.M. DRANCHUK

Permission is hereby granted to the NATIONAL LIBRARY OF CANADA to microfilm this thesis and to lend or sell copies of the film.

The author reserves other publication rights, and neither the thesis nor extensive extracts from it may be printed or otherwise reproduced without the author's written permission.

L'autorisation est, par la présente, accordée à la BIBLIOTHÈQUE NATIONALE DU CANADA de microfilmer cette thèse et de prêter ou de vendre des exemplaires du film.

L'auteur se réserve les autres droits de publication; ni la thèse ni de longs extraits de celle-ci ne doivent être imprimés ou autrement reproduits sans l'autorisation écrite de l'auteur.

DATED/*DATÉ* October 2, 1974 SIGNED/*SIGNÉ* J.D. McFarland

PERMANENT ADDRESS/*RÉSIDENCE FIXÉ* #1510, 1200 6 ST SW.
CALGARY, ALBERTA T2R 1H3

NL-91 (11-73)

THE UNIVERSITY OF ALBERTA

TRANSITION TO TURBULENCE IN POROUS MEDIA

by

James D. McFarland

A THESIS

SUBMITTED TO THE FACULTY OF GRADUATE STUDIES AND RESEARCH

IN PARTIAL FULFILLMENT OF THE REQUIREMENTS FOR THE DEGREE

OF MASTER OF SCIENCE IN PETROLEUM ENGINEERING

DEPARTMENT OF MINERAL ENGINEERING

EDMONTON, ALBERTA

FALL, 1974

THE UNIVERSITY OF ALBERTA

FACULTY OF GRADUATE STUDIES AND RESEARCH

The undersigned certify that they have read, and recommend to the Faculty of Graduate Studies and Research, for acceptance, a thesis entitled "Transition to Turbulence in Porous Media" submitted by James D. McFarland in partial fulfillment of the requirements for the degree of Master of Science in Petroleum Engineering.

.....

Supervisor

.....

.....

Date .....

ABSTRACT

Flow experiments were conducted on four synthetic porous media in order to determine the Reynolds number at the transition to turbulent flow. Two sphere sizes were used, of 0.25 and 0.5 in. diameter, and two packing arrangements, a Cubic No. 1 and an Orthorhombic No. 2.

The streaming birefringence visualization technique was used to observe the transition to turbulence in flowing milling yellow dye solutions. The technique offers the advantage of eliminating the flow disturbance that results when intrusive measuring techniques are employed, and provides good reproducibility and sharp definition of the transition.

The non-Newtonian nature of the birefringent milling yellow dye solution required that the effective viscosity in the Reynolds number at the transition to turbulence be calculated from the Forchheimer equation adapted for non-Newtonian flow. This method proved to give satisfactory results based on a comparison of the effective viscosity versus superficial velocity curves developed from the sphere pack flow data with the apparent viscosity versus shear rate curve measured directly on the Weissenberg rheogoniometer.

The results indicate that the transition to turbulent flow takes place over a range of Reynolds numbers from 0.241 to 4.56, where the Reynolds number is based on superficial velocity and a length parameter equal to the product of the permeability and the inertial resistance coefficient of the pack. These results compare favourably with those in the literature when a Reynolds number based on superficial velocity and sphere diameter is used for this comparison.

ACKNOWLEDGEMENTS

The author wishes to express his thanks to Professor P.M. Dranchuk for his advice and understanding in the supervision of this project.

Special thanks are due to the personnel of the former Department of Chemical and Petroleum Engineering Machine Shop, whose invaluable assistance in constructing the equipment made this study possible.

The author wishes to express appreciation to many individuals in the former Department of Chemical and Petroleum Engineering for their helpful suggestions, and in particular, to Dr. F.A. Seyer, and Mr. Y. Senturk and Mr. R. Hlede.

Special acknowledgements are made to the National Research Council of Canada, who awarded the author scholarship funds for a two year period, as well as supplying the funds for equipment construction.

The author wishes to express his gratitude to his wife, Valerie, whose understanding and continued encouragement made completion of this study possible.

TABLE OF CONTENTS

LIST OF TABLES

LIST OF FIGURES

LIST OF PHOTOGRAPHIC PLATES

INTRODUCTION

In predicting fluid flow behavior in porous media, it is important to determine the type of flow regime that will be present, whether it be viscous, inertial or turbulent, or some intermediate type. This in turn will assist in determining which of the Darcy, Forchheimer or some higher order equation, will be applicable to predicting the flow behavior. The range of a particular flow regime should be defined for this purpose, by means of a parameter constructed of readily measureable quantities. In this study, it is proposed to define the upper limit of the laminar flow region by means of a Reynolds number. This limit is the transition to turbulence and will be determined by means of the streaming birefringence visualization technique.

The early literature attributed deviations from Darcy's law at high flow rates to both inertial effects and to the onset of turbulence. However, the work of many researchers, including Schneebeli (1), Chauveteau and Thirriot (2), Jones (3), Dudgeon (4) and Wright (5), has indicated that contrary to that which takes place in a pipe, the pressure drop in a porous medium ceases to be a linear function of the flowrate well before the appearance of turbulence. The transition from Darcy's law is due to the increasing importance of inertial effects in a flow regime that remains steady at this transition. Turbulence, which is characterized by unsteady motion, sets in at higher velocities. The Forchheimer equation has been used successfully in the region beyond the applicability of the Darcy equation but with no defined upper limit.

The transition to turbulence, like the upper limit of validity of Darcy's law, has been characterized in the literature by means of a Reynolds number. The types of porous media used in these studies and the definitions of the Reynolds number vary widely. In general, results have shown that a range of Reynolds numbers exist at which turbulence develops, depending on the type of porous medium used and the measuring points within the porous medium. However, it might be hoped that with a better definition of the Reynolds number, a single Reynolds number or a very narrow range of Reynolds numbers might be obtained at the transition to turbulence.

The most popular techniques used in the determination of the transition to turbulence in packed beds have been firstly, the injection of a dye stream into the pack in order to observe unsteady motion and secondly, the insertion of a probe into the pack in order to obtain hot wire anemometer measurements of velocity fluctuations. However, both methods are less than satisfactory. Dye streams quickly discolour the flowing fluid making visual studies difficult. Any object placed in a pore space necessarily affects the flow regime in that pore space. A review of available visualization techniques suggested that the streaming birefringence technique could be useful in packed bed studies. The technique requires only a fluid that exhibits birefringence and a polarized light source. Shear patterns within the fluid are readily discernible as is the transition to unsteady motion of these patterns. No upset of the flow regime is necessary. However, certain complications are introduced.

In order to observe birefringence, a colloidal suspension of some type of particle is required with the result that the rheological

properties of the fluid are non-Newtonian. Proper interpretation of the pressure drop - flowrate data is required in order to define an effective viscosity for use in a Reynolds number at the transition to turbulence. The requirement to extrapolate non-Newtonian flow behavior to Newtonian flow behavior is the most serious deficiency of the streaming birefringence visualization technique.

Another limitation of this visualization technique is the requirement that the depth of the flow field not be so great as to cause excessive interference of the shear patterns. In order to meet this requirement and the requirement to compare this work with that of different authors, as well as to more clearly define the specific effects of particle geometry, it was decided to use well defined arrays of spheres as the porous media in this study.

THEORY

Visco-Inertial Flow and the Transition to Turbulence

It has long been recognized that Darcy's law is valid only in a certain seepage velocity region in porous media, outside of which more general flow equations are required. According to Scheidegger (6), Forchheimer suggested that Darcy's law should be modified at high velocities by including a second-order term in the velocity and proposed the following for linear horizontal incompressible flow:

$$-\frac{\Delta p}{\Delta x} = a\,q + b\,q^2 \qquad (1)$$

where p is the pressure, x is the length dimension, q is the superficial velocity and a and b are constants. As Scheidegger (7) has indicated, the Forchheimer equation was postulated from semi-theoretical reasoning by analogy with the phenomena occurring in pipes. However, the equation was shown to have a sound mechanistic basis by Chwyl (8). He derived it from the Navier-Stokes equation in the form used by Green and Duwez (9). When integrated for the linear horizontal incompressible flow case, this equation yields

$$-\frac{\Delta p}{\Delta x} = F_A\,\mu\,q + F_B\,\rho\,q^2 \qquad (2)$$

where μ is the fluid viscosity, ρ is the fluid density and F_A and F_B are constants independent of fluid properties. The constants F_A and F_B,

having only the dimensions of length, characterize the structure of the porous medium and have been referred to as the viscous and inertial resistance coefficients of the porous medium. Since the viscous resistance coefficient F_A, is the inverse of the permeability k, Eq. 2 can be written as

$$-\frac{\Delta p}{\Delta x} = \frac{1}{k}\mu q + F_B \rho q^2 \tag{3}$$

Equation 3 indicates that as the velocity increases the losses due to the inertia of the fluid become much more important. The gradual transition from the Darcy region is marked by the increasing importance of these inertia losses as compared to the losses due to viscous shear.

By definition, the Reynolds number is the ratio of the inertial forces to the viscous forces. Green and Duwez (10) then, defined the Reynolds number in a porous medium as

$$Re = \frac{F_B \rho q}{F_A \mu} \tag{4}$$

or

$$Re = \frac{k F_B \rho q}{\mu} \tag{5}$$

In order to compare the results of this study with others in the literature, the following form of the Reynolds number will be used:

$$Re_D = \frac{D \rho q}{\mu} \tag{6}$$

where D, is the average sphere or particle diameter.

A common means of correlation in the literature is the friction factor versus Reynolds number plot as developed for porous media by Fancher, Lewis and Barnes (11). As indicated by Green and Duwez (12), the ratio of "dissipative" forces to the inertial forces defines the friction factor and for a linear horizontal incompressible system described by Eq. 3

$$C_f = \frac{-\frac{1}{F_B}\frac{\Delta p}{\Delta x}}{\frac{\rho q^2}{2}} \tag{7}$$

where C_f is the friction factor. Ahmed and Sunada (13) removed the factor of 2 in the friction factor, and based on an equation similar to Eq. 3, derived the following relationship:

$$F = \frac{-\frac{1}{F_B}\frac{\Delta p}{\Delta x}}{\rho q^2} = \frac{1}{Re} + 1 \tag{8}$$

where $F = C_f/2$.

At some higher velocity, turbulent motion will occur. Equation 3 should be applicable up to that point based on the comments as to the mechanistic basis of the equation. Much effort has been directed in the literature to the determination of the transition to turbulence, primarily to discount the theory that departures from Darcy's law are due to the onset of turbulence. The results of these studies will be used for comparative purposes to validate the technique used in this study.

Schneebeli (14) used a dye tracer technique in two packs, one consisting of a dumped bed of 27 mm spheres and the other consisting of

1 in. gravel, to establish the transition to turbulence at about Re_D 60.

Jolls and Hanratty (15) measured the instantaneous rate of mass transfer at different positions on the surface of a sphere in a dumped bed of 1 in. glass spheres. They obtained a range of Reynolds numbers at the transition to turbulence of Re_D 110-150 which was confirmed with dye tracer studies.

Chauveteau and Thirriot (16) created a two dimensional model of a porous medium consisting of arbitrary shapes separated by channels of various configurations, designed specifically for visual studies. By means of a dye tracer technique they observed a transition to turbulence in some pores at Re_D 80 and observed turbulence in all pores at Re_D 180. The diameter used in the Reynolds number was a hydraulic diameter.

Wegner, Karabelas and Hanratty (17) used the dye tracer technique in a cubic pack of 3 in. spheres to establish a transition to turbulence in the range Re_D 90-120.

Kyle and Perrine (18) created two dimensional models of porous media in order to facilitate visual studies. Their models consisted of a matrix of 0.5 in. cylinders arranged in three patterns to obtain three different porosities. By means of a dye tracer technique they established a transition to turbulence in the range Re_D 55-137, depending on the pack porosity, where the length parameter in the Reynolds number was the cylinder diameter.

Kingston and Nunge (19) in a recent study used a hot wire anemometer to measure the transition to turbulence in a rhombohedral array of 1.5 in. spheres. They determined a transition to turbulence in the range Re_D 80-200.

Streaming Birefringence

A birefringent material is one which exhibits different propagation velocities for optical vibrations in different internal planes which are parallel to the direction of propagation (20). Certain pure liquids and colloidal suspensions, though isotropic at rest, become birefringent or double refracting to the passage of light when a preferred orientation is imposed on the molecules or suspended particles by external forces (21).

In pure liquids, measureabl[illegible]fringence is obtainable only with very high shear rates, and so colloidal suspensions are normally used for flow visualization (22). When the flowing fluid is viewed by transmitted polarized light, optical interference patterns are observed composed of alternate light and dark bands. In steady laminar flow these patterns are stationary, but in turbulent flow they take on a random, eddying motion. This behavior affords an excellent qualitative method for the study of laminar, transition and turbulent flow.

The phenomenon of streaming birefringence has been used extensively; from the investigation of car body design (23) to the simulation of blood flows in prosthetic circulatory-assist devices (24). These applications produced qualitative results only, but provided valuable insights into the nature of flow fields that are bounded by complex geometries (25). A great deal of effort has been directed to obtaining reliable quantitative information from the technique, but the drawbacks appear substantial (26), not the least of which, is the requirement for two dimensional flow.

The optical theory of streaming birefringence as applied to the

fluid polariscope, the apparatus used in flow studies, is essentially the same as that applied to photoelastic stress analyses in solids. The two volume work of Frocht (27) and the short description by Redner (28) can be referred to for this purpose. The theory enables one to determine the stress distribution in a two dimensional model by defining the magnitude and direction of the two principal stresses. This can be done by passing plane polarized light through the model and observing the two types of lines formed. One type is called an isochromatic, which is coloured when white light is used, and which is related to the magnitude of the difference between the principal stresses in the liquid at a particular point. The other is an isoclinic, which is black, and which is related to the direction of the principal stresses. It may be advantageous to observe isochromatics separately and for this purpose monochromatic circularly polarized light is used.

In a fluid in motion, the principal stresses are the effective shear stresses due to velocity differences across the direction of flow. The isochromatics show the relative magnitude of these shear stresses, and as a result, may be regarded as stream paths within the fluid (29).

In the past, many colloidal suspensions have been used to observe streaming birefringence including solutions of vanadium pentoxide, bentonite, benzopurpurin, sesame oil and milling yellow dye. Prados and Peebles (30) reviewed many of the early studies prior to 1959 and determined that aqueous solutions of milling yellow dye provided superior results.

The visual quality of the interference patterns is primarily a function of three factors: (i) solution concentration, (ii) temperature,

and (iii) depth of the flow field. Preparation of a solution that will exhibit any birefringence at all, is a very tedious task involving extensive trial and error. At high temperatures, the intensity of birefringence diminishes, likely due to the action of Brownian motion on the suspended particles (31). Design of the flow model may require some compromise in order that brighter colour and definition can be obtained from a small depth of flow field.

For qualitative purposes, streaming birefringence is a valuable tool. However, the technique does have a serious deficiency. Colloidal suspensions are normally non-Newtonian in nature. Included in this group are aqueous solutions of milling yellow dye, the rheological data of which are described adequately by the Powell - Eyring relationship for pseudoplastic materials over a range of deformation rates of 50-10,000 sec^{-1} (32). The difficulty arises when non-Newtonian fluid behavior is extrapolated directly to describe Newtonian fluid behavior.

Non-Newtonian Flow Behavior in Porous Media

A pseudoplastic or shear thinning fluid exhibits three more or less distinct regions in its rheological behavior, as follows:

1. A region of Newtonian behavior at low shear rates characterized by a limiting constant viscosity.
2. A non-linear region characterized by a range of decreasing apparent viscosities - a non-Newtonian region.

3. A region of Newtonian behavior at high shear rates again characterized by a constant, but smaller, viscosity.

Much effort has been directed to the prediction of non-Newtonian, and in particular pseudoplastic behavior, in porous media, and to the correlation of porous media experimental results with viscometric data. This activity has arisen with the increasing interest in the use of polymers as mobility control agents in waterflood schemes. Gogarty (33), Christopher and Middleman (34), Sadowski and Bird (35), McKinley Jahns and Harris (36), and Gregory and Griskey (37), examined the rheological properties of pseudoplastics in porous media and developed equations to predict their behavior. Other authors extended these investigations to studies of anomalous effects at high shear rates (38,39,40,41,42), and to the incorporation of polymer flow behavior in reservoir simulation (43).

Savins (44), in his state of the art review of non-Newtonian flow in porous media, has classified the scale-up methods used to establish a pressure drop - flowrate relationship into four broad categories, the most widely used of which, are the following two:

1. Couple a particular model of the porous medium with a functional relationship between shear rate and shear stress for the fluid.

2. Adapt Darcy's law to non-Newtonain fluids without invoking a particular model of the purely viscous

behavior of the fluid, even though Darcy's law is strictly applicable to Newtonian fluids only.

As far as the author could ascertain, in all cases, effective viscosities determined for correlation purposes from experimental data in porous media, have been calculated using Darcy's law. Jennings, Rogers and West (45) did establish a flow equation that incorporated viscous, inertial and elastic effects, with which they proposed to analyze experimental non-Newtonian flow data in various types of porous media. However, in calculating the effective viscosity, the inertial term was deleted - it being assumed to be relatively insignificant.

In order to incorporate the inertial effects in the calculation of effective viscosity, Eq. 3 can be rewritten to yield the following equation that applies to pseudoplastic fluid flow in porous media:

$$\mu_e = -\frac{k}{q}\frac{\Delta p}{\Delta x} - k F_B \rho q \qquad (9)$$

where μ has been replaced by μ_e, the effective viscosity, which is a function of the shear rate.

EXPERIMENTAL DESIGN

Prior to undertaking any fabrication of equipment, several design considerations had to be investigated. These were made necessary, in part, by the nature of the flow visualization technique. These can be separated into those that relate to the bead pack design and those that relate to the flow system design.

Bead Pack Design

As noted by Kyle and Perrine (46), the complicated three dimensional structure of porous materials has made detailed visual studies very difficult. They opted to develop a two dimensional staggered cylinder model to simulate the behavior of a three dimensional porous medium in which visual studies of the transition to turbulence could be made with ease. Chauveteau and Thirriot (47) constructed a two dimensional model of different character, but for the same purpose. Although the streaming birefringence visualization technique requires a two dimensional flow regime for quantitative work, qualitative results are obtainable in a three dimensional system if the effects in the third dimension, the depth of the flow field, do not unduly interfere.

In order to reduce the depth of flow field and to create a sufficient pore size in which to observe the flow regime, systematic sphere packs, two layers in depth, were chosen for study. Two sphere sizes, of 0.25 in. and 0.5 in. diameter, and two packing arrangements, a Cubic No. I and an Orthorhombic No. 2 in the terminology of Graton

Fraser (48), were chosen to make up the four packs used in this study. Kingston and Nunge (49) have suggested that consistent use of a single well defined geometry in well defined arrays would simplify the comparison of the work of different authors and more clearly define the specific effect of changes in geometry.

In any packed bed studies with a limited depth of flow, the importance of wall effects is of interest. As Dudgeon (50) points out, the flow rates measured in a dumped bed of spheres, for example, are taken to represent those that would apply to one dimensional flow in an infinite medium under the same potential gradient. Of course, this is not strictly correct since the walls of the container distort the velocity distribution across the bed from the uniform distribution that would be present in an infinite medium. This effect can be attributed to two things; firstly, the higher porosity at the wall in a dumped bed, and secondly, the zero fluid velocity at the wall. The obvious technique to eliminate the porosity effect in a systematic sphere packing arrangement is to use half and quarter spheres at the container walls. This has become standard practice (51,52,53,54). In effect, one obtains the configuration of Graton and Fraser's unit cell (55) at the wall, the unit cell being defined as follows: it is bounded by planes so passed through the centres of adjacent spheres, that the resulting polyhedral form meets the requirement of being the smallest possible sample that will completely represent the manner of packing and void distribution throughout the body of which it is a part.

For the packs used in this study, it was decided to recess the spheres to half their diameter into the walls of the pack, as opposed

to attaching half spheres to the walls.

Though the effect of zero velocity at the wall is probably minor compared to the porosity effect, Mickley, Smith and Korchak (56) have measured 10% higher velocities at one particle diameter from the wall than in the centre of a Rhombohedral No. 3 array. They concluded that the wall itself decreases the total resistance to flow in the wall region. The momentum transfer associated with the presence of a wall appears to be less than that which occurs when opposing streams enter a void. Van der Merwe and Gauvin (57) have interpreted the absence of this effect in a Cubic No. 1 pack as showing that uniformity of flow is achieved only when the symmetry of the packing at the wall does not impose physically unrealistic flow behavior. The blocked void passages of the Rhombohedral No. 3 array at the container wall then, would upset the uniformity of flow. Much less than a 10% error in the measured superficial velocities should be expected in the cubic and orthorhombic packs of this study. The symmetry of the packing at the wall in these packs should not cause unrealistic flow behavior.

End effects may be an important consideration depending on where pressure measurements are taken along the pack length. Van der Merwe and Gauvin (58) measured drag coefficients along the length of a bead pack and concluded that only at seven or eight sphere banks downstream of the pack entrance, are end effects eliminated. The effect of the downstream end of the packing does not extend more than one sphere bank back into the pack.

In this study, it was decided to set pressure taps at least eight banks downstream of the entrance and four banks upstream of the exit.

Flow System Design

The other area of concern was the flow system design, the major consideration being the effect that any pulsations in the flow might have on the observed flow patterns.

There were two types of systems considered: firstly, a simple system using a centrifugal pump, pumping directly into the bead pack, and secondly, a constant head gravity feed system. Miller (59) questioned the use of a centrifugal pump, pumping directly to the visualization section in streaming birefringence studies, since he observed pulsations in the flow at the pump frequency.

In this study, any masking of the start of unsteady flow was undesirable, so that the constant head gravity feed system was chosen. Any pulsations from the centrifugal pump are damped by the reservoir tank that it is feeding.

Another consideration in the design of the components of the flow system was the effect that certain metals have on the stability of milling yellow dye solutions. Miller (60) indicated that copper, brass and lead cause changes in the properties of the solution, primarily through early precipitation of the dye particles. He suggested that a flow system consisting chiefly of stainless steel, plastic and glass would not cause changes in the physical properties of the milling yellow dye solution.

Because of the temperature and concentration sensitivity of the properties of milling yellow dye solutions, controlled conditions are necessary. This requires that evaporation be minimized by fitting tight lids on all tanks, and that a temperature controller be used.

APPARATUS

As discussed in the previous section, two packing arrangements, a Cubic No. 1 and an Orthorhombic No. 2, and two sphere sizes, of 0.25 in. and 0.5 in. diameter, were used to construct four packs. The packs were constructed with 1 in. lucite plate. The spheres were precision stainless steel ball bearings (±0.001 in. tolerance). In order to recess each layer of balls to half their diameter in each plate, a programmable drill press was used to drill a grid of holes on D + 0.005 in. centres. This spacing of holes was required to allow ease in fitting the balls to the drilled holes. The 0.5 in. pack consisted of a two layer 10 by 27 array and the 0.25 in. pack, a two layer 20 by 60 array. Each pack was fitted with a flow diffuser consisting of a thin lucite plate drilled with holes, placed just upstream of the balls. For the 0.5 in. packs, pressure taps were drilled 8 banks downstream of the entrance to the array and 4 banks upstream of the exit. For the 0.25 in. packs, pressure taps were drilled 16 banks downstream of the entrance and 8 banks upstream of the exit. Figure 1 illustrates a section from each packing arrangement which is also the unit cell for each arrangement.

The flow system was a constant head, gravity feed system as illustrated in Fig. 2. The materials used for components of the system included PVC piping, PVC valves except for one brass needle valve, a 316 stainless steel centrifugal pump and polyethylene tanks. A 30 ft. head was available in the large scale projects laboratory of the former Department of Chemical and Petroleum Engineering by placing

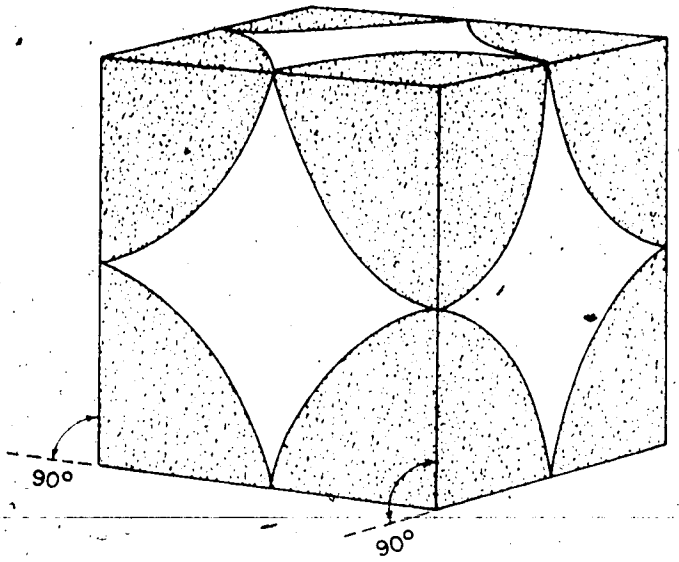

CUBIC NO. 1

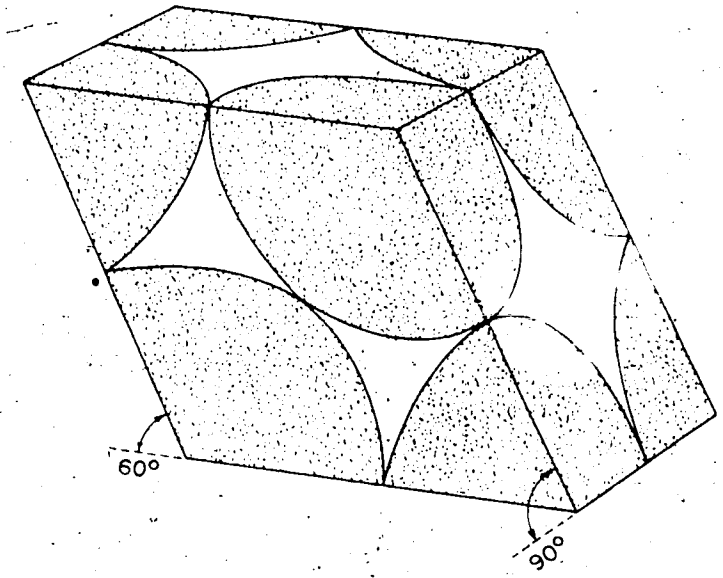

ORTHORHOMBIC NO. 2

FIG. 1. UNIT CELLS FOR PACKING ARRANGEMENT TYPES

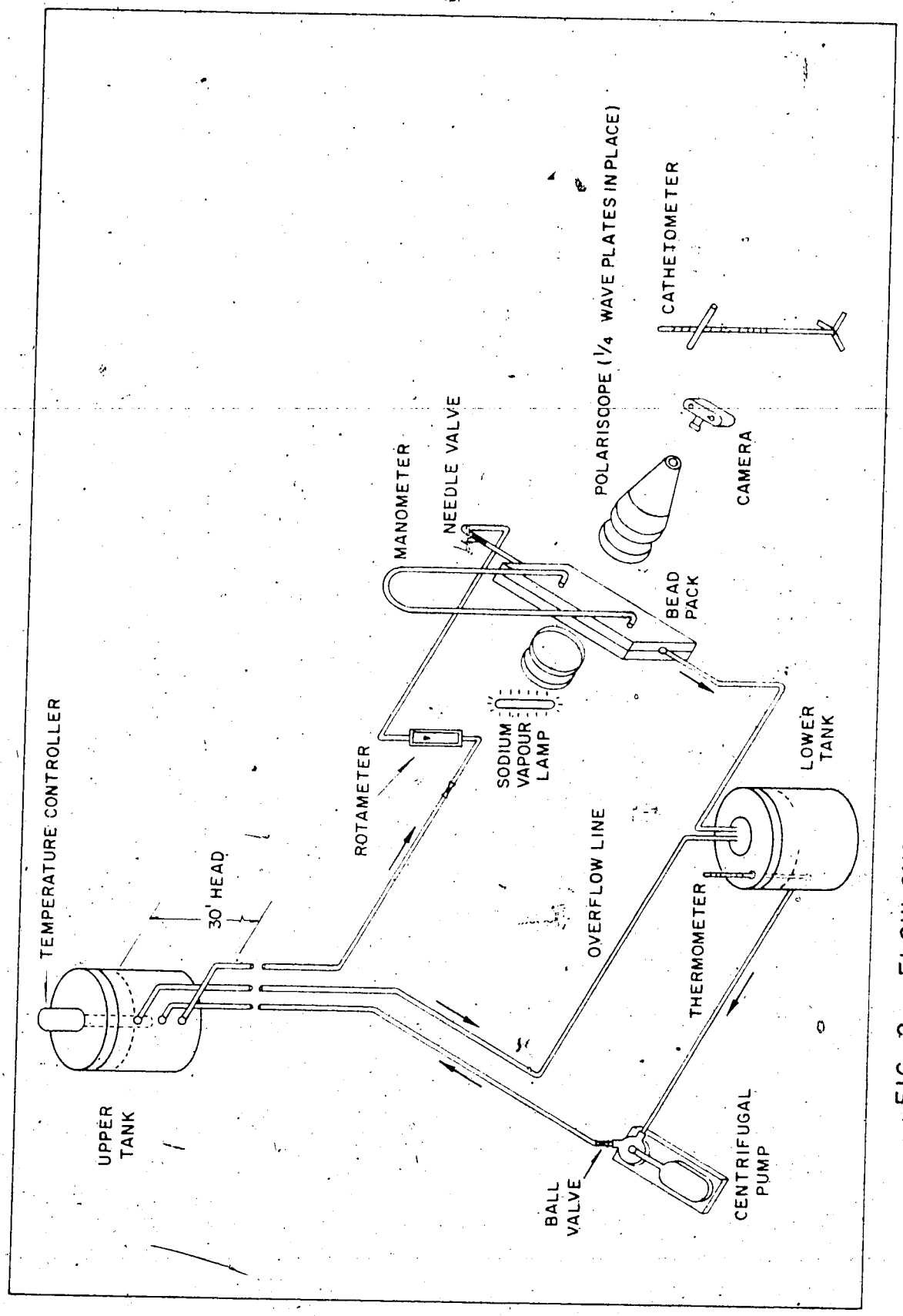

FIG. 2. FLOW SYSTEM LAYOUT WITH POLARISCOPE IN PLACE

a tank on a higher floor. The pump used to maintain the fluid in this upper tank was a Hayward - Gordon model AA centrifugal pump equipped with a 0.75 h.p. motor. The temperature controller was equipped with a 1,000 watt heating element, and was fitted to the upper tank. Flowrates were measured with two rotameters, one covering the range 0-85 gm/sec, and the other covering the range 50-150 gm/sec. Pressure drops were measured with an inverted, 100 cm manometer, using the flowing fluid because of the small pressure drops involved. Fluid level differences in the arms of the manometer were measured with a cathetometer, consisting of a travelling telescope on a graduated post (resolution ±0.005 cm).

The polarized light source consisted of a Sharples 5.5 in. diameter, combined transmission and diffuse light polariscope. The diameter of the polarizer, analyzer and quarter wave plates were such that most of the width of the packed bed could be viewed. The polariscope was equipped with a camera mount, and a magnification capability by means of a lens system behind the analyzer. Black and white photographs of the flow patterns visible in polarized light were taken with a Miranda camera (105 mm, F3.5) using a high contrast film (Copex).

PROCEDURES

Preparation of Milling Yellow Dye Solution

Efforts of other researchers have indicated that preparation of any suspension that will exhibit suitable birefringent behavior is a tedious task. In this study, the work of Muraoka (61) has been used as a guide.

A working volume of about 75 liters of milling yellow-dye solution was required. The following method was used to prepare this volume in 2 liter batches. Two liters of a 31% by volume, glycerine - distilled water solution was prepared. This volume was placed in a 5 liter distillation flask, to which was added 38 gm of Keco Acid Milling Yellow 8NG (Keystone Aniline and Chemical Co., Inc., Chicago, Illinois). In addition, 2.68 gm of a chelating agent, EDTA*, was added prior to boiling the solution at total reflux for one hour. Boiling stones were used to reduce bumping, and the entire apparatus placed inside a fume hood behind safety glass, to minimize the danger of an unexpected bump. The solution was then allowed to cool for at least one hour, was carefully filtered with a suction system and the resulting clear solution was placed in capped glass containers. This process was repeated over 37 times to make up the 75 liter working volume.

The rheological properties of the solution were measured at 30°C (±1°C) on a Weissenberg rheogoniometer. Density measurements over the temperature range 29-31°C (±0.1°C) were made in the Standards Laboratory of the former Department of Chemical and Petroleum Engineering, The University of Alberta.

* (ethylenedinitrilo)tetracetic acid

Measurement of k and F_B of Bead Packs

Prior to making any runs with the non-Newtonian milling yellow dye solution, it was necessary to establish the bead pack parameters, k and F_B, with a Newtonian fluid. The fluid used for this purpose was a 66% by weight, glycerine-distilled water solution totalling about 75 liters. Density and kinematic viscosity data were measured over the temperature range 27-31°C (±0.1°C) in the Standards Laboratory of the former Department of Chemical and Petroleum Engineering, The University of Alberta.

The rotameters were first calibrated with this solution at a temperature of 30.3°C (±0.1°C). By trial and error, it was determined that this temperature could be maintained for long periods of time with the temperature controller used. Volumes of solution passing through the rotameter in a given time period were weighed in order to establish a calibration curve of mass flowrate versus rotameter reading. Two trials were made at each rotameter reading.

The aqueous glycerine solution was then circulated through the system until a stabilized temperature of 30.3°C (±0.1°C) was obtained by suitable adjustment of the temperature controller. The manometer was then attached to the pressure taps and pressure drop - flowrate data obtained through a sequence from low to high rates. The needle valve just upstream of the bead pack was used to control the rate. About 10 minutes was required to obtain a constant fluid level in the lower tank, and in turn, the upper tank supplying the constant head, by manipulation of the ball valve just downstream of the pump. This procedure was repeated for each pack.

Determination of the Reynolds Number at the Transition to Turbulence

The rotameters were again calibrated, this time with the milling yellow dye solution, at a temperature of 30.3°C (±0.1°C). The polariscope apparatus was then arranged such that circularly polarized monochromatic light could be produced. Isochromatics alone appear in this arrangement. This involved using quarter wave plates at the polarizer and analyzer, and a sodium vapour lamp as a monochromatic light source. The camera was aligned with the end of the analyzer lens and focused.

The milling yellow dye solution was circulated through the system until a stabilized temperature of 30.3°C (±0.1°C) was obtained. Pressure drop - flowrate data were then obtained over a range of flowrates that went just beyond the transition to unsteady motion. The flowrate at this transition, as indicated by the first unsteady motion of the isochromatic pattern, was measured several times as a check on reproducibility. This procedure was repeated for each pack.

Photographs of the isochromatic pattern were taken at several rates, both above and below the start of unsteady motion. Several camera aperture and shutter speed readings were used at each rate in order to ensure that a photograph of high contrast could be obtained. The exposed Copex film was developed in a Neofin Blue solution for maximum contrast.

Treatment of Data

A linear least squares program was written in order to obtain estimates of the bead pack parameters k and F_B in Eq. 3 from the

aqueous glycerine, pressure drop - flowrate data.

The pressure drop - flowrate data of the milling yellow dye solution, obtained as H, the head loss between the pressure taps, versus W, the mass flowrate, were first smoothed by eye. The effective viscosity μ_e, was calculated from Eq. 9 at several superficial velocities with the pressure drop as obtained from the smoothed data. A curve of μ_e versus q was thus constructed for each pack. An effective viscosity was determined from the μ_e versus q curve at the superficial velocity at which turbulence was first observed. The Reynolds number at this point was then calculated from Eq. 5 using the k and F_B determined previously.

RESULTS

Bead Pack and Fluid Properties

The physical properties of the aqueous glycerine and the milling yellow dye solutions are given in Table 1. The rheological behavior of the milling yellow dye solution at 30.3°C (±1°C) is illustrated in Fig. 3, a curve of apparent viscosity μ_a, versus the shear rate $\dot{\gamma}$, obtained on a Weissenberg rheogoniometer. Note that the constant viscosity end points were not completely defined since the rheogoniometer cones required to reach very low and very high shear rates were not available at the time. However, an extrapolation to the constant viscosity at low shear rates is indicated.

The physical properties of each of the four bead packs are illustrated in Table 2, where A is the cross-sectional area of the pack, and X is the distance between the pressure taps. Note that the porosities listed have not been measured, but are the ideal porosities for the particular packing arrangements.

The experimental and processed pressure drop - flowrate data obtained with the aqueous glycerine solution are tabulated in Tables A.1 through A.4 in the Appendix, along with a sample calculation. The rotameter calibration curves used are illustrated in Figs. A.1 and A.2 in the Appendix. Values of $\Delta p/\Delta x$ and q, along with the least squares fit to Eq. 3, are plotted in Figs. 4 through 7. Table 3 is a tabulation of the values of k and F_B, along with the 95% confidence limits on each parameter, as obtained for each pack from the least squares fittings indicated in Figs. 4 through 7.

TABLE 1. PHYSICAL PROPERTIES OF AQUEOUS GLYCERINE AND MILLING YELLOW DYE SOLUTIONS

	ρ $(\frac{GM}{CM^3})$ @ 30.3 ± 0.1°C	μ (POISE) @ 30.3 ± 0.1°C
Aqueous Glycerine Solution	1.1877	0.1018
Milling Yellow Dye Solution	1.0628	$\mu_a = f(\dot{\gamma})$

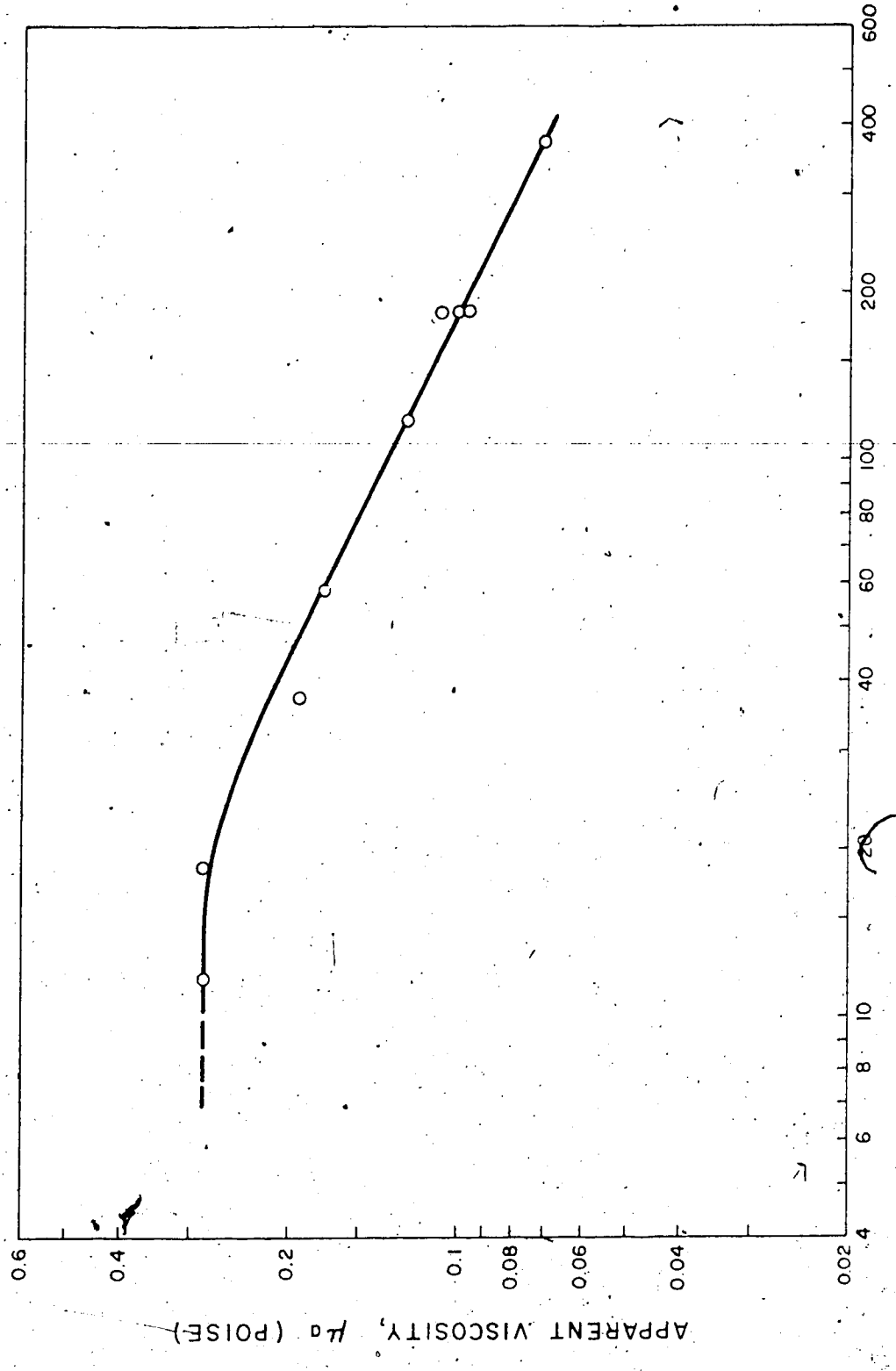

FIG. 3. MILLING YELLOW DYE SOLUTION μ_a vs $\dot{\gamma}$ CURVE

TABLE 2. PHYSICAL PROPERTIES OF BEAD PACKS

PACK NO.	PACKING TYPE	D (IN.)	POROSITY (%)	A (CM^2)	X (CM)
1	Cubic No. 1	0.5	47.64	16.419	20.384
2	Orthorhombic No. 2	0.5	39.54	15.041	17.971
3	Cubic No. 1	0.25	47.64	8.218	20.130
4	Orthorhombic No. 2	0.25	39.54	7.117	20.130

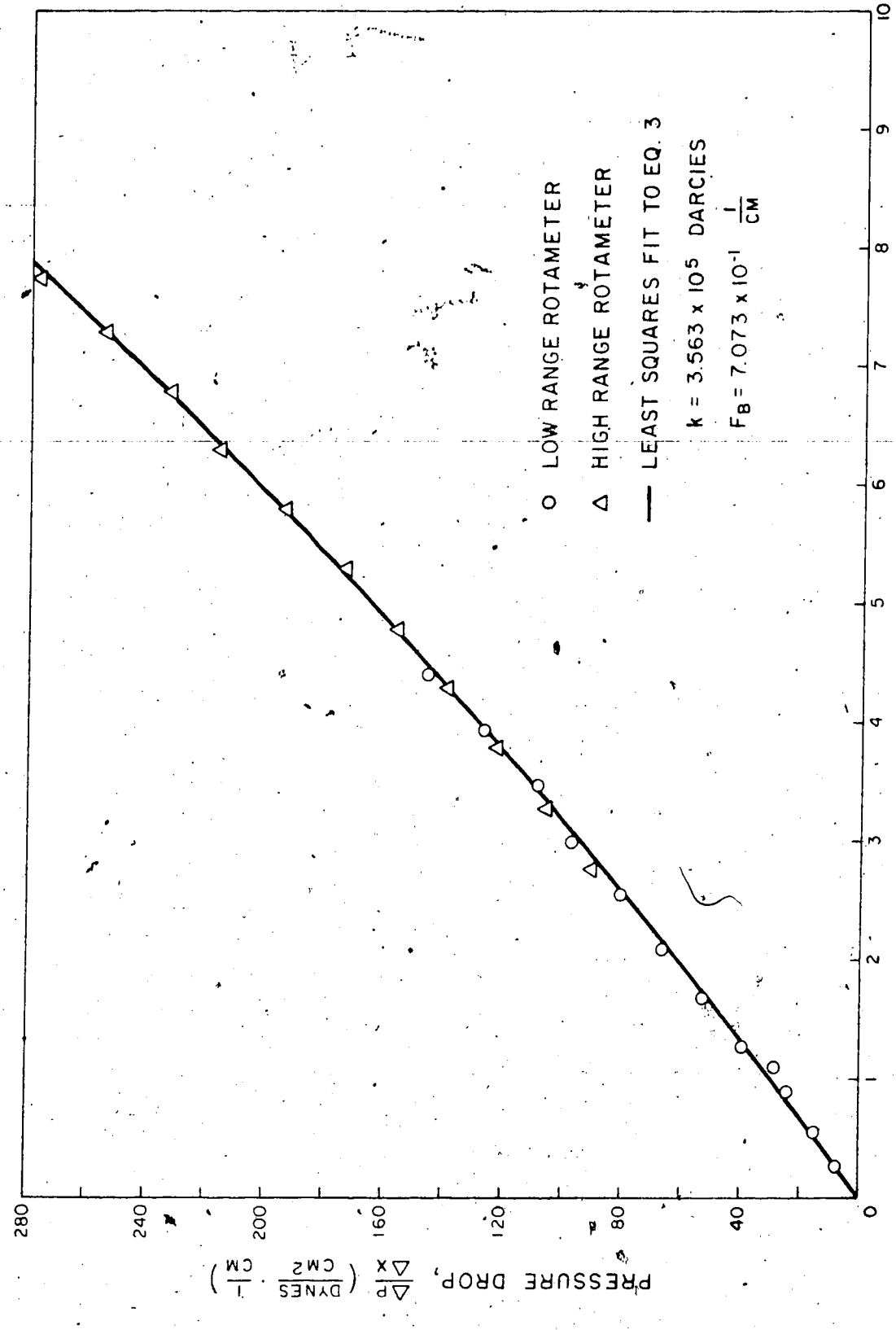

FIG. 4. AQUEOUS GLYCERINE SOLUTION $\Delta p/\Delta x$ vs q DATA AND LEAST SQUARES FIT FOR PACK NO. 1

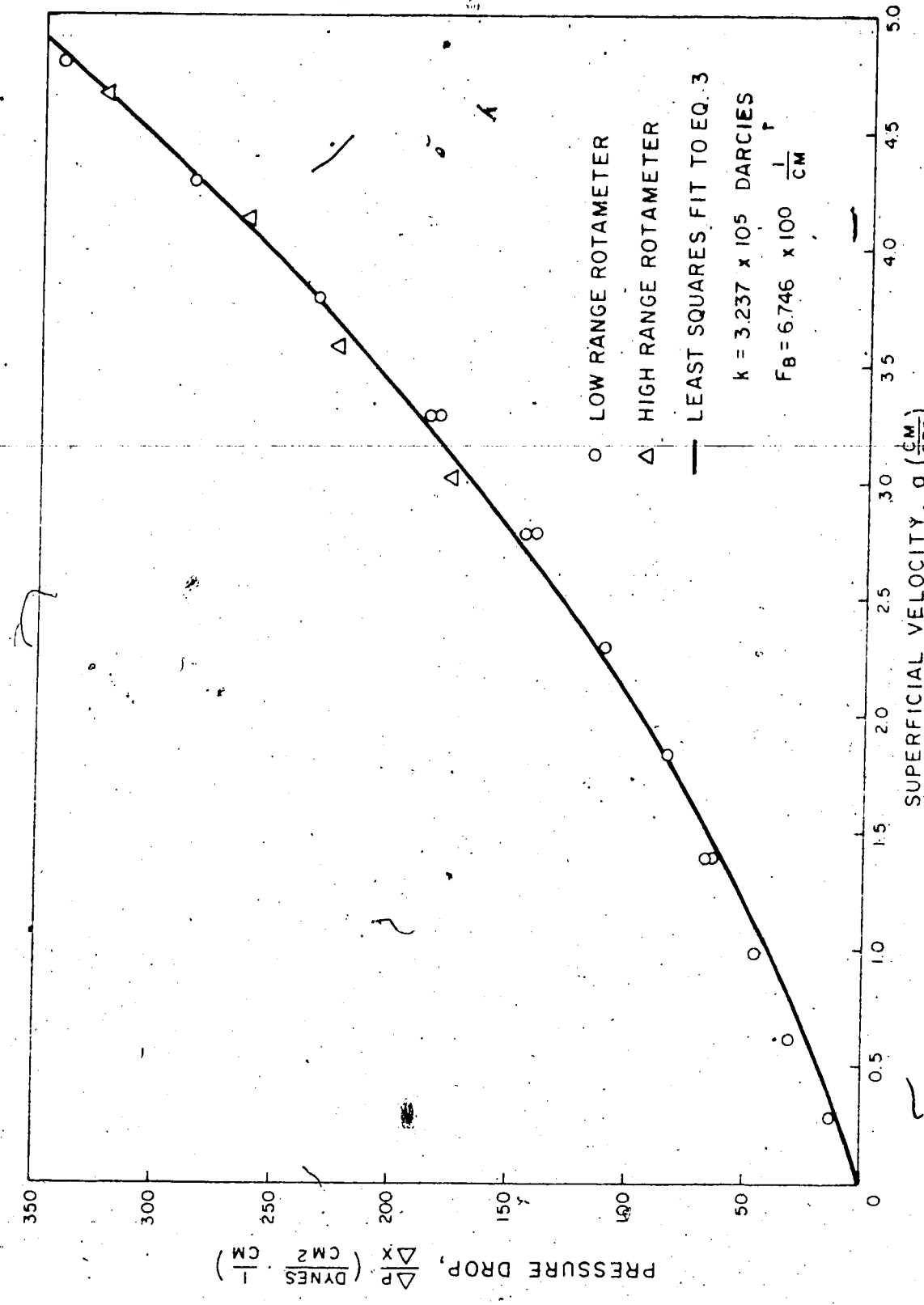

FIG. 5. AQUEOUS GLYCERINE SOLUTION $\Delta p/\Delta x$ vs q DATA AND LEAST SQUARES FIT FOR PACK NO. 2

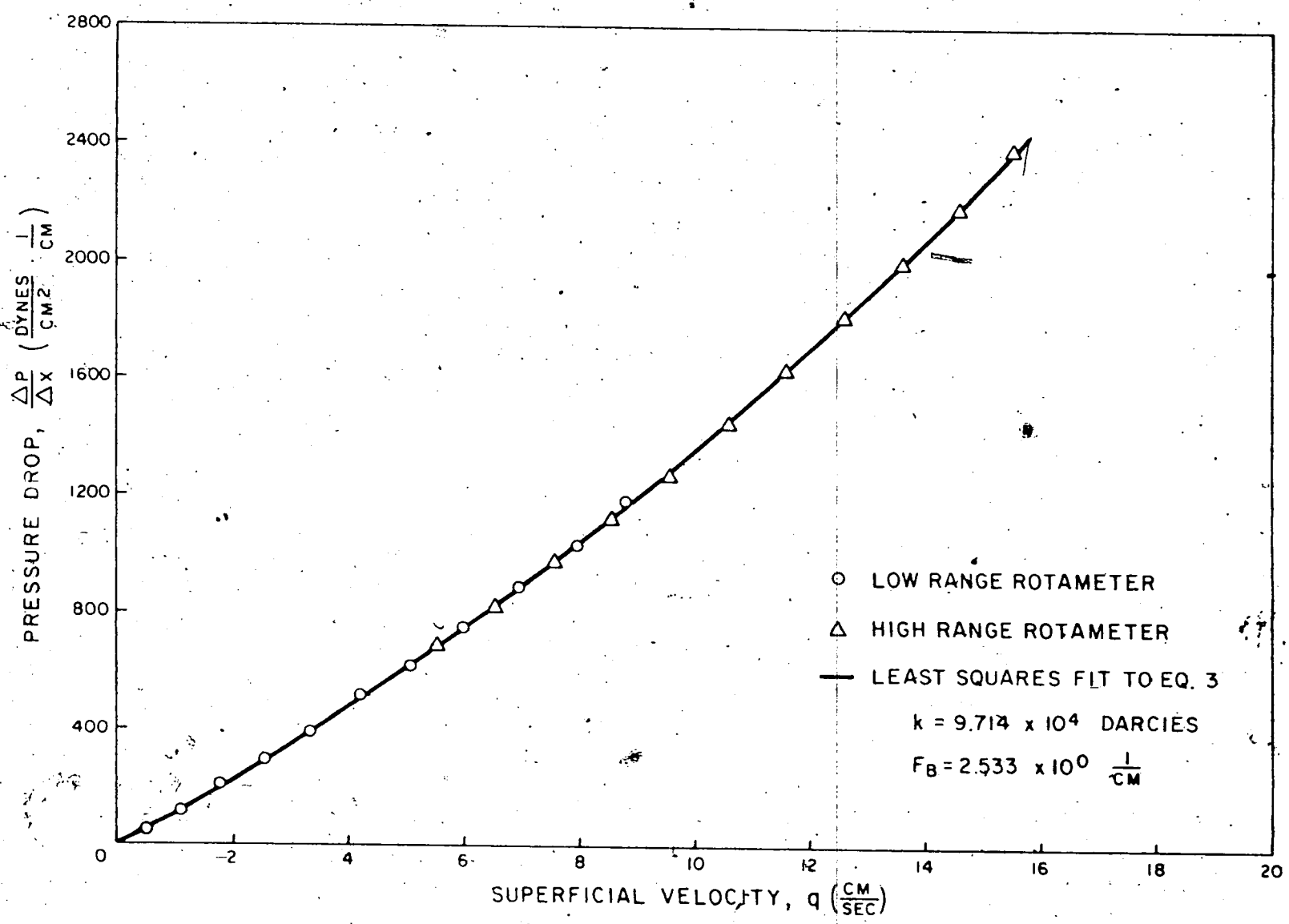

FIG. 6: AQUEOUS GLYCERINE SOLUTION $\Delta p/\Delta x$ vs q DATA AND LEAST SQUARES FIT FOR PACK NO. 3

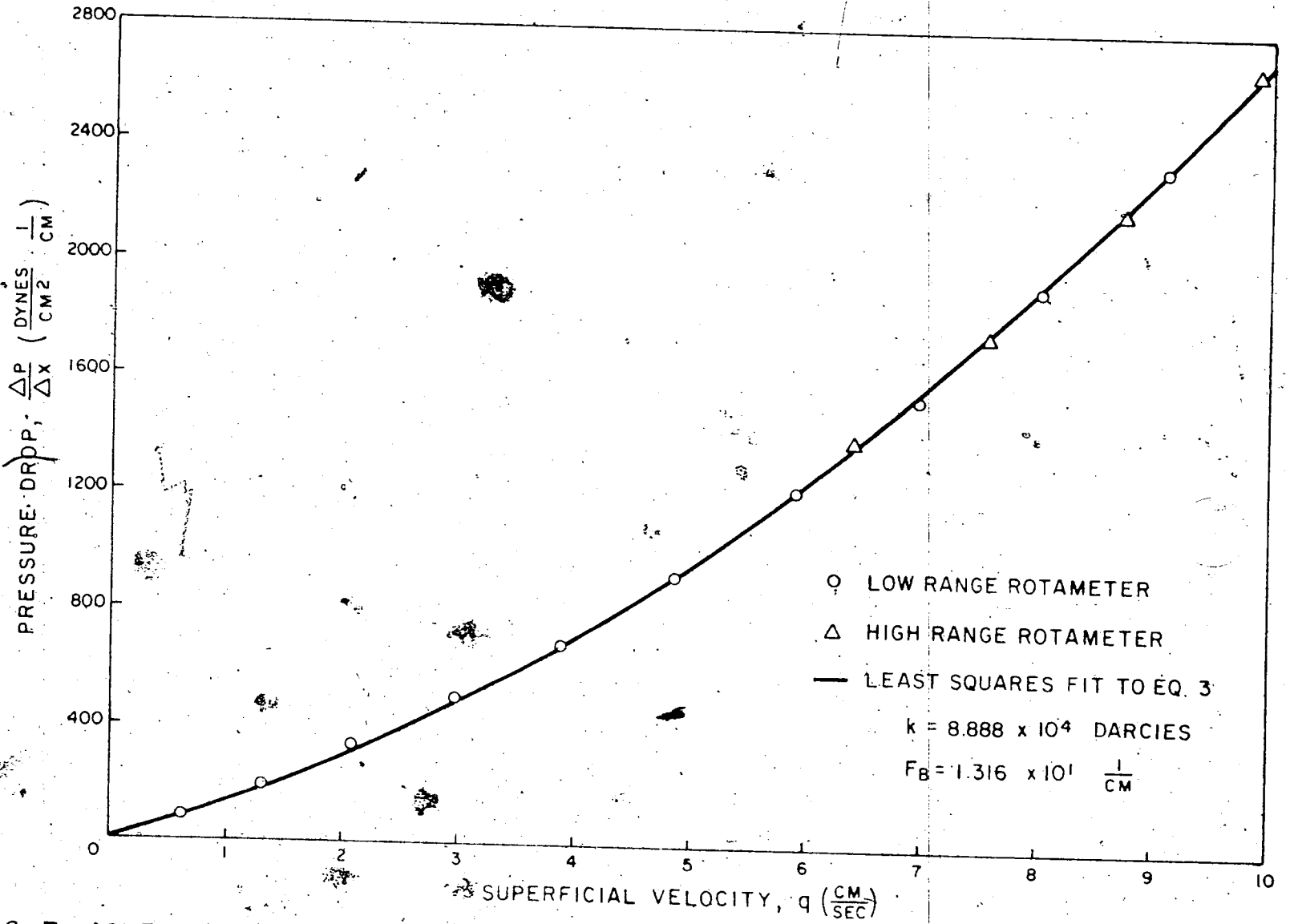

FIG. 7. AQUEOUS GLYCERINE SOLUTION $\Delta p/\Delta x$ vs q DATA AND LEAST SQUARES FIT FOR PACK NO. 4

TABLE 3. PACK PARAMETERS k AND F_B AND 95% CONFIDENCE LIMITS

PACK NO.	PARAMETERS 95% CONFIDENCE LIMITS k (DARCIES)	F_B $(\frac{1}{CM})$
1	$(3.563\pm0.063)\times10^{5}$	$(7.073\pm0.729)\times10^{-1}$
2	$(3.237\pm0.419)\times10^{5}$	$(6.746\pm0.887)\times10^{0}$
3	$(9.714\pm0.150)\times10^{4}$	$(2.533\pm0.117)\times10^{0}$
4	$(8.888\pm0.466)\times10^{4}$	$(1.316\pm0.061)\times10^{1}$

Transition to Turbulence

Values of the experimental and processed, head loss and mass flowrate data obtained with the milling yellow dye solution are tabulated in Tables A.5 through A.8 in the Appendix. Values of the head loss H, versus mass flowrate W, along with eye-fit curves, are plotted in Figs. 8 through 11. Tables A.9 through A.12 in the Appendix indicate the points chosen from the fitted curves in Figs. 8 through 11, from which values of μ_e were calculated with Eq. 9. Figures 12 through 15 illustrate the μ_e versus q curves obtained by this process for each pack.

The value of the superficial velocity q, at which turbulence was first observed in each pack is indicated in Figs. 12 through 15. The Reynolds numbers at these transition superficial velocities, as calculated from Eq. 5, are tabulated in Table 4. Values of μ_e required in the calculation of these Reynolds numbers were obtained from Figs. 12 through 15 and are tabulated in Table 4.

Figure 16 illustrates the modified friction factor F, versus Reynolds number Re, relationship for the aqueous glycerine solution data. These data are tabulated in Tables A.1 through A.4 in the Appendix. The Reynolds numbers at the transition to turbulence in each pack, as determined from the milling yellow dye solution flow studies, are also indicated in Fig. 16.

Photographs of the isochromatic patterns visible in the flowing milling yellow dye solution experiments conducted on Pack No. 1, for Reynolds numbers both above and below the onset of turbulence, are illustrated in Plate 1.

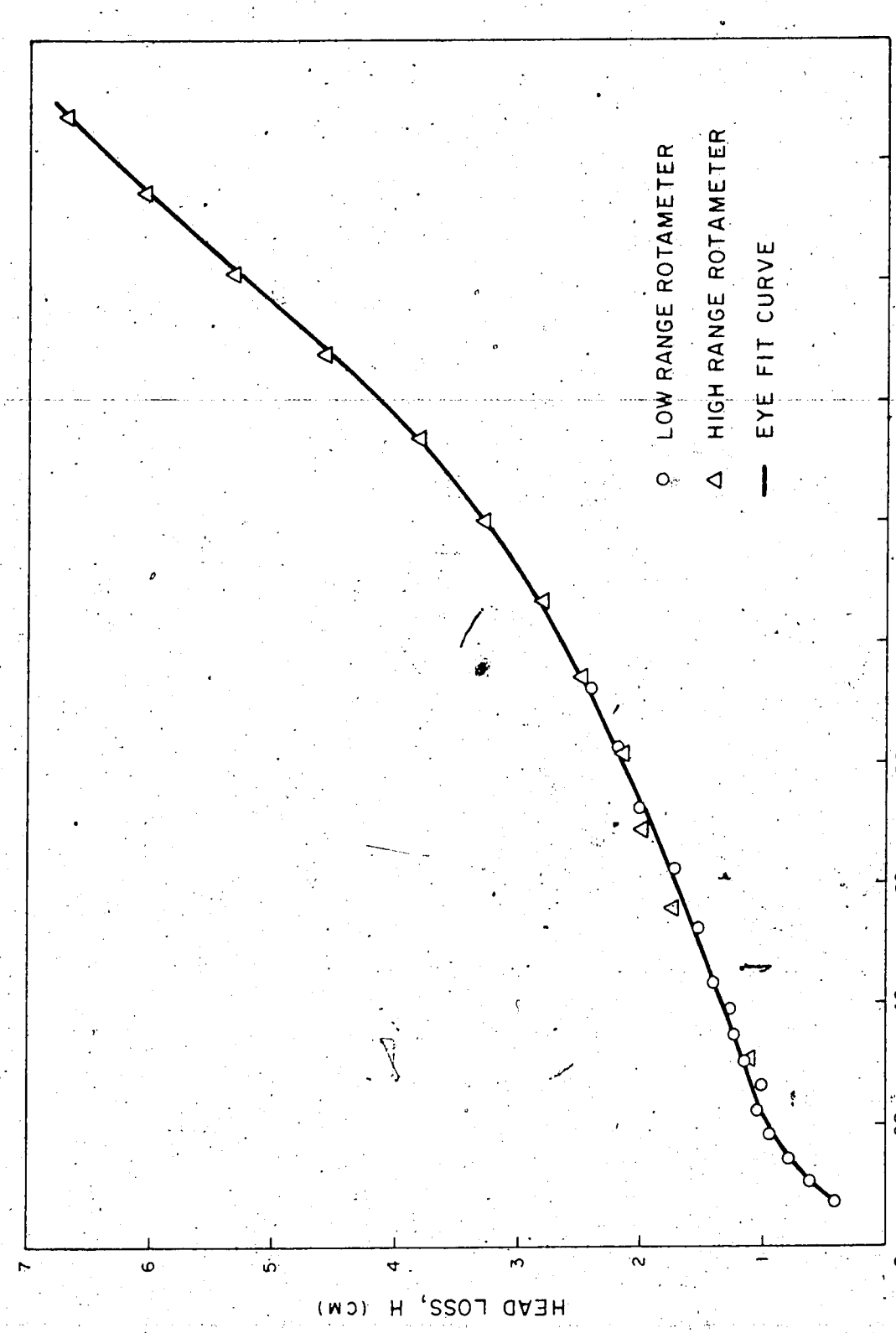

FIG. 8. EXPERIMENTAL MILLING YELLOW DYE SOLUTION H vs W DATA FOR PACK NO. 1

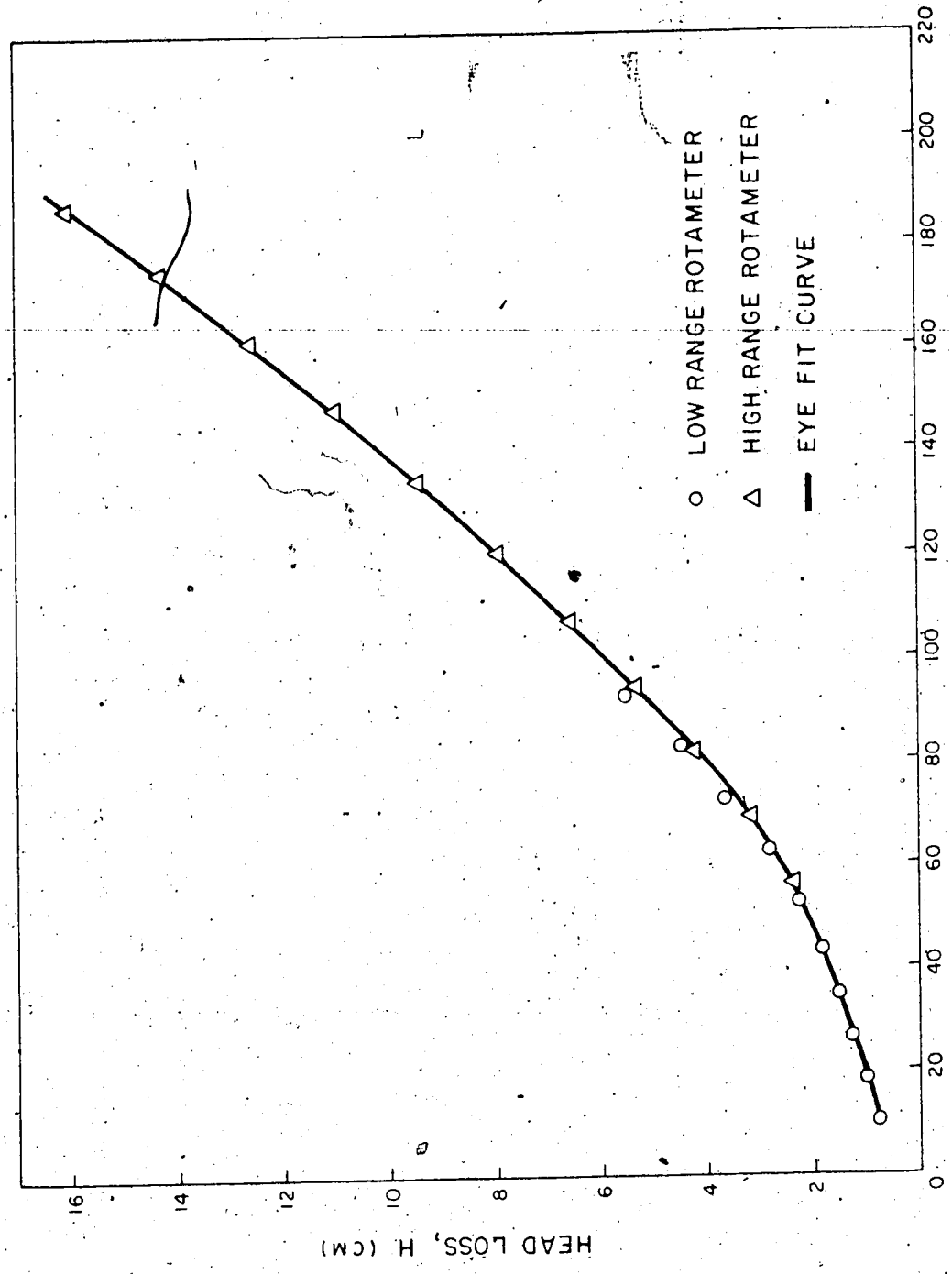

FIG. 9. EXPERIMENTAL MILLING YELLOW DYE SOLUTION H vs W DATA FOR PACK NO. 2

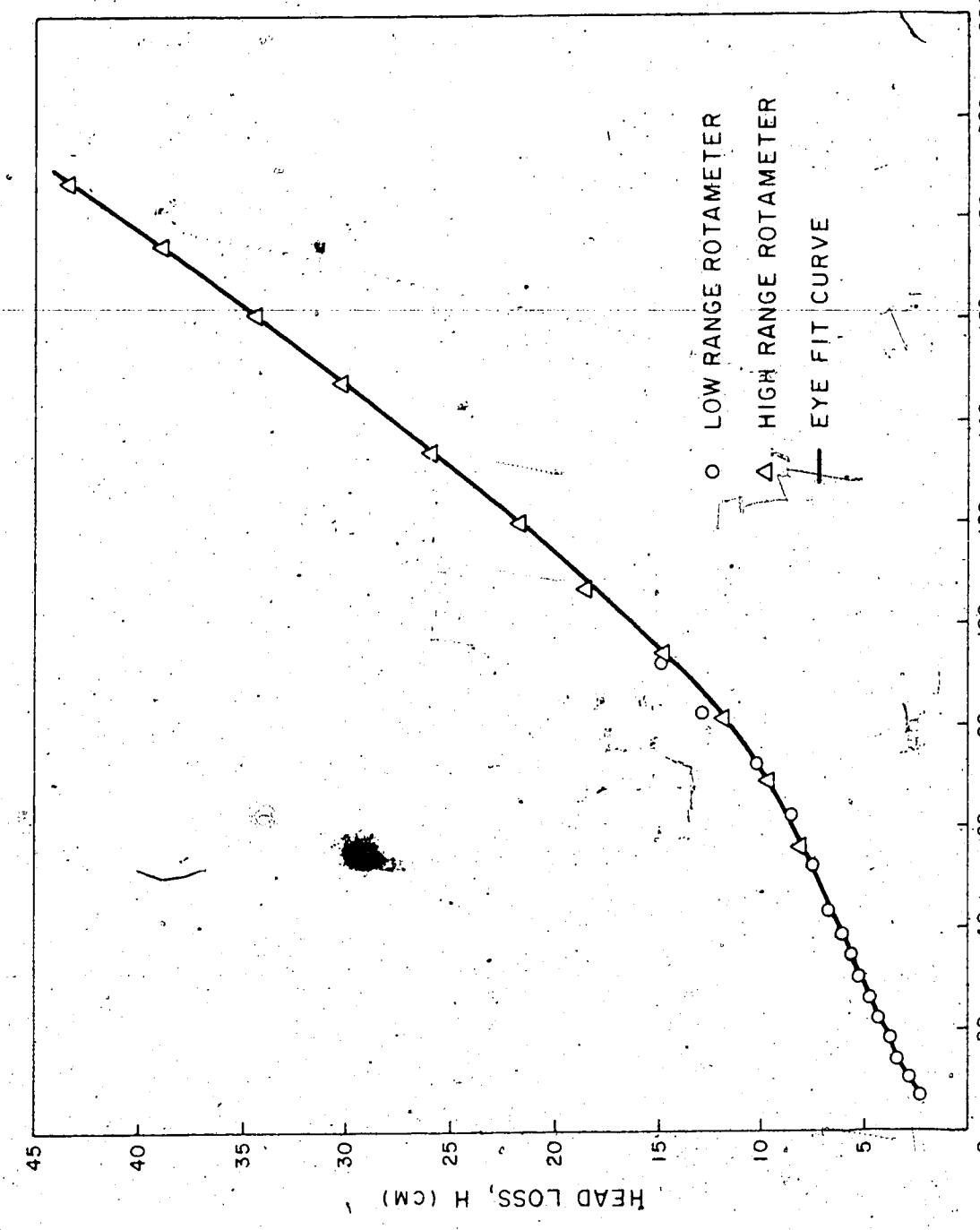

FIG. 10. EXPERIMENTAL MILLING YELLOW DYE SOLUTION H vs W DATA FOR PACK NO. 3

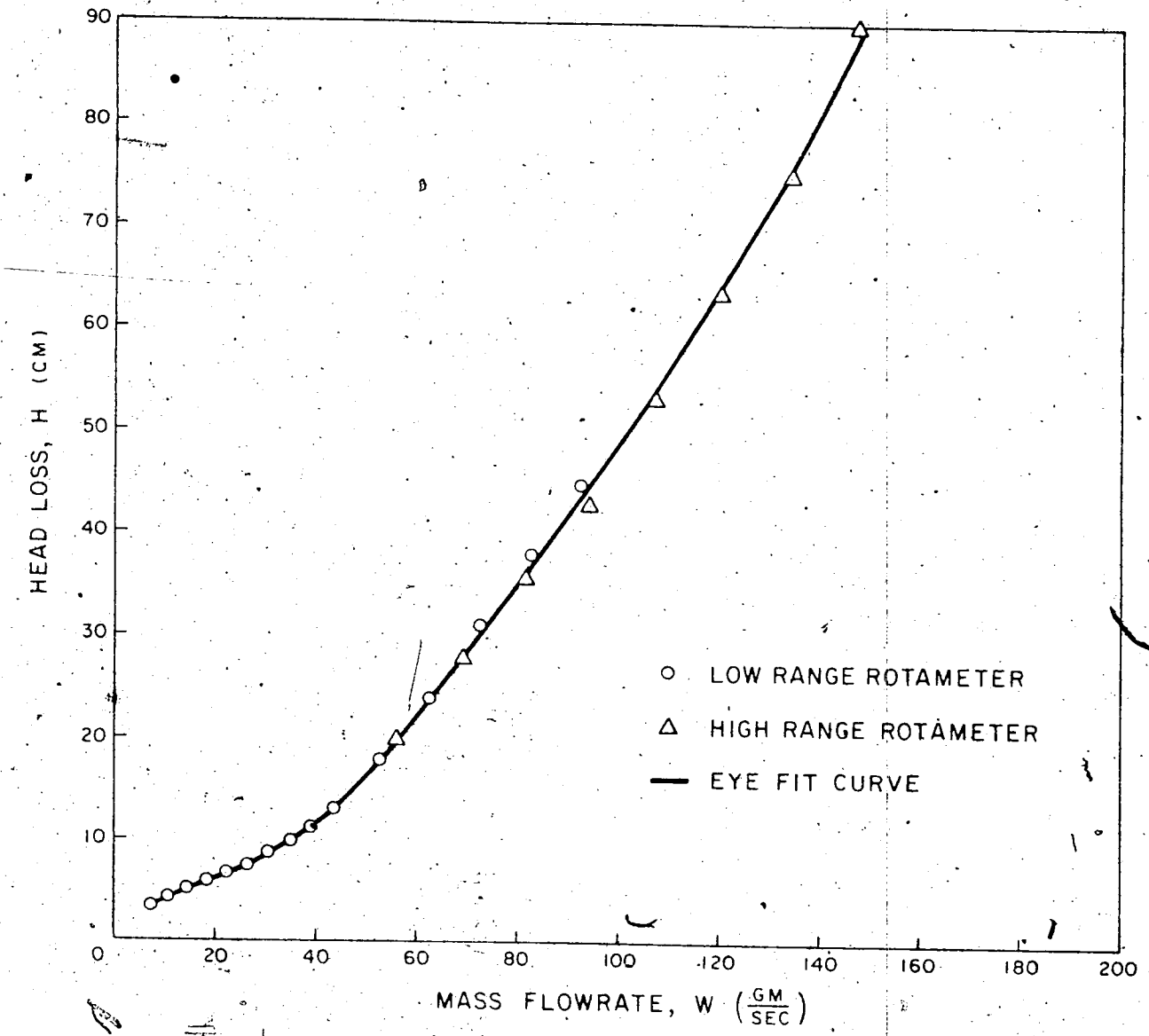

FIG. 11. EXPERIMENTAL MILLING YELLOW DYE SOLUTION H vs W DATA FOR PACK NO. 4

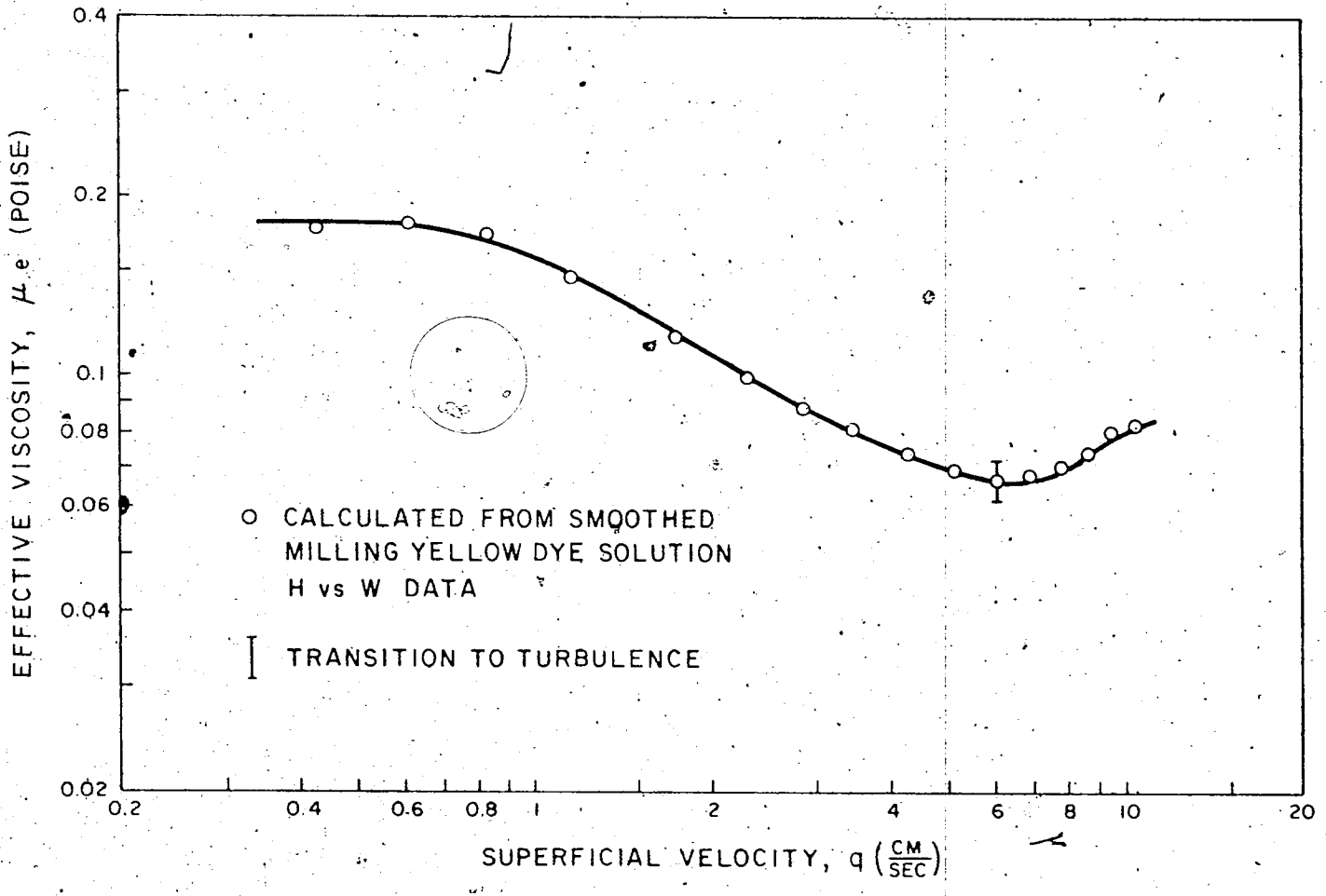

FIG. 12. MILLING YELLOW DYE SOLUTION μ_e vs q CURVE FOR PACK NO. I

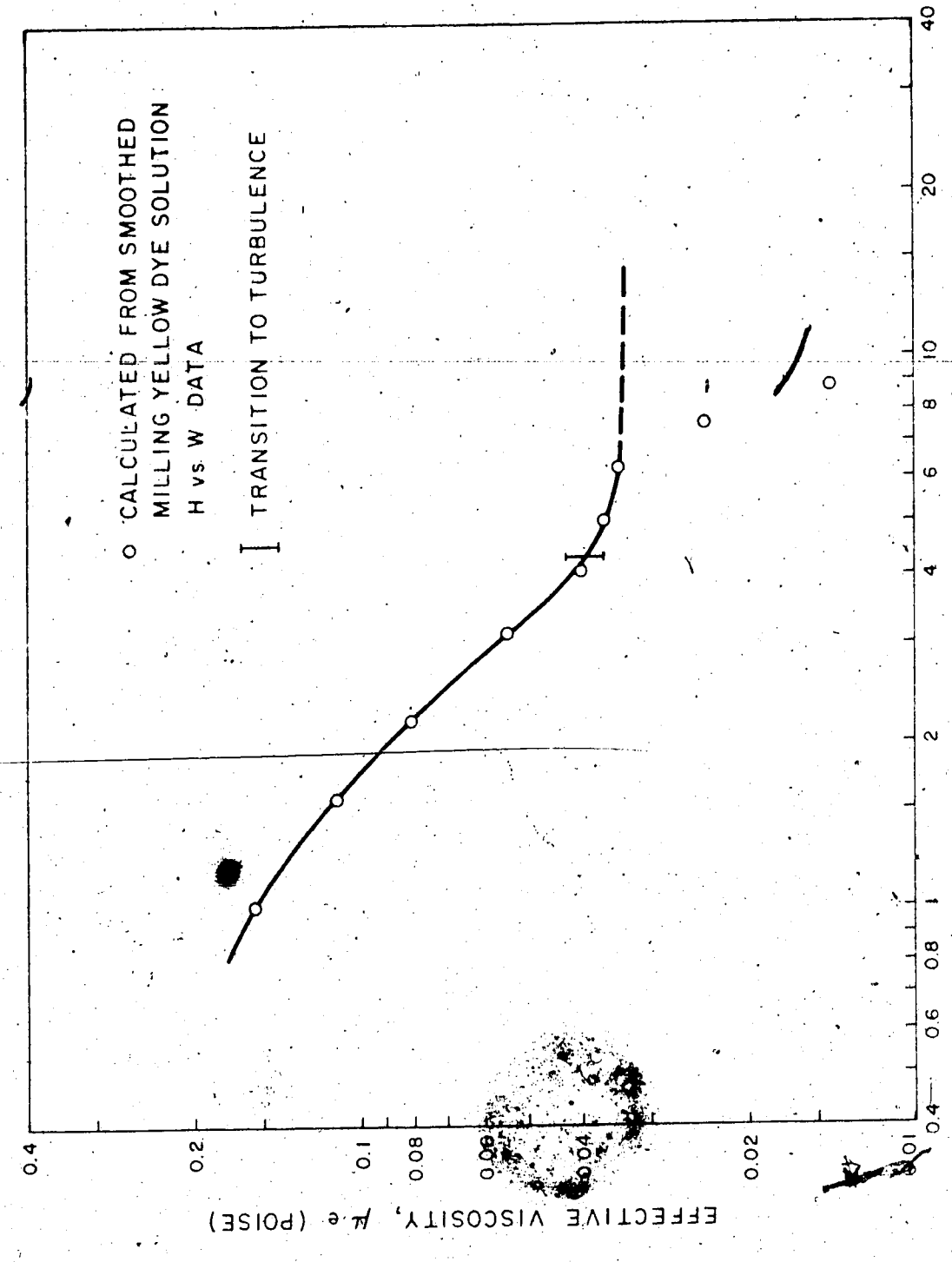

FIG. 13. MILLING YELLOW DYE SOLUTION μe vs q CURVE FOR PACK NO. 2

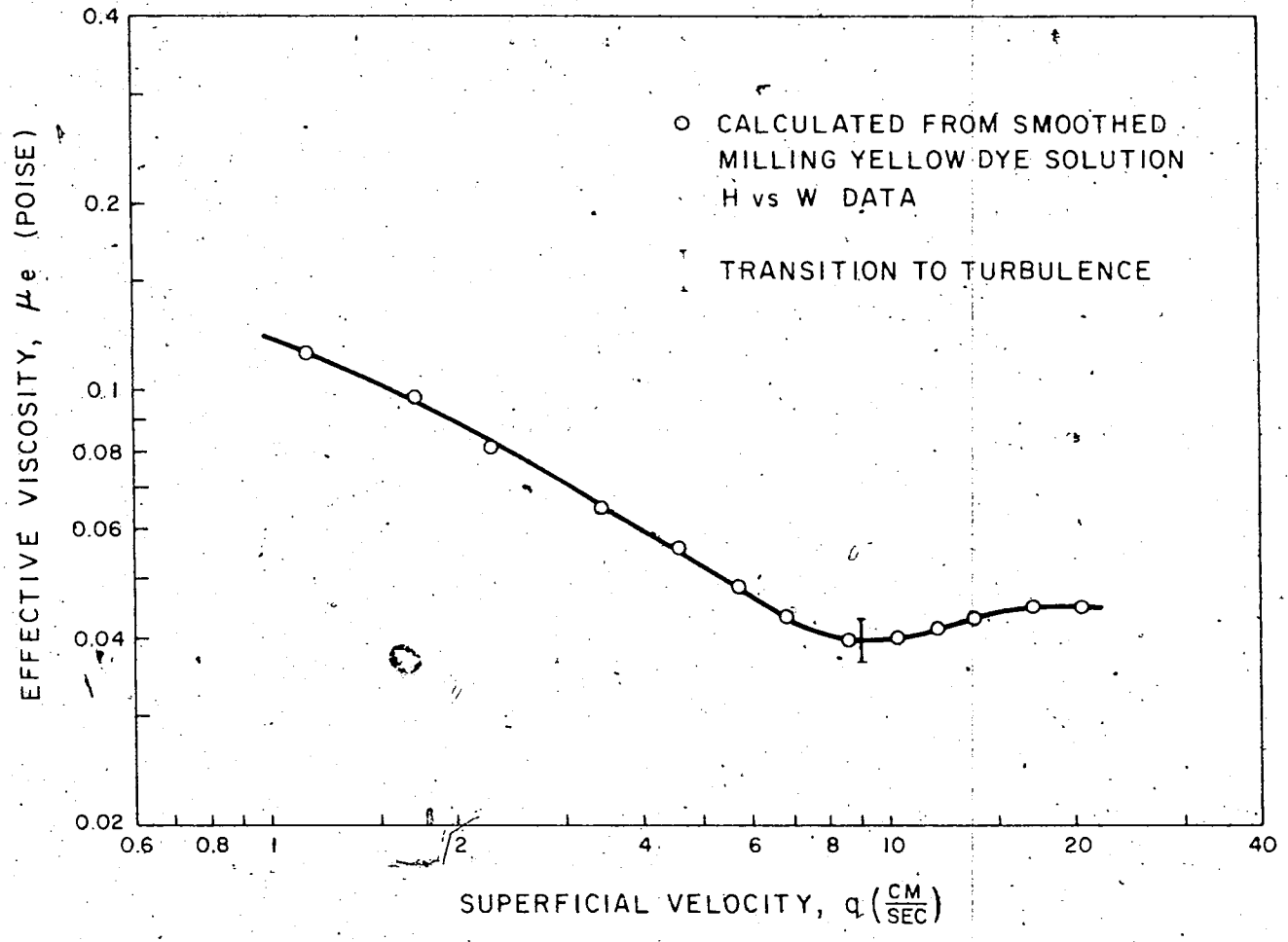

FIG. 14. MILLING YELLOW DYE SOLUTION μe vs q CURVE FOR PACK NO. 3

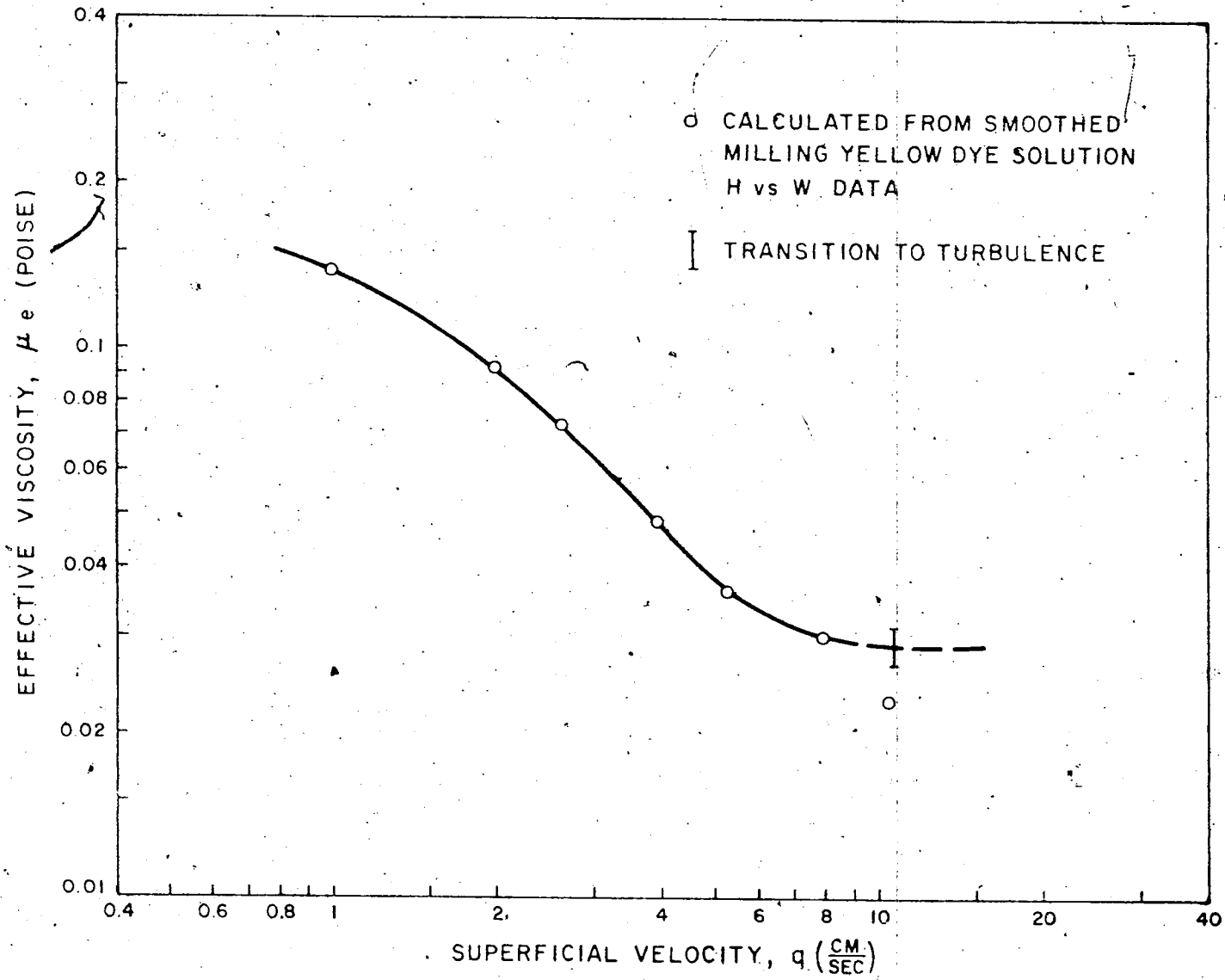

FIG. 15. MILLING YELLOW DYE SOLUTION μe vs q CURVE FOR PACK NO. 4

TABLE 4. VALUES OF q, μ_e AND Re FOR EACH PACK AT THE TRANSITION TO TURBULENCE

PACK NO.	PACKING TYPE	D (IN.)	VALUES AT THE TRANSITION TO TURBULENCE q ($\frac{CM}{SEC}$)	μ_e (POISE)	Re
1	Cubic No. 1	0.5	6.075	0.0665	0.241
2	Orthorhombic No. 2	0.5	4.285	0.0395	2.49
3	Cubic No. 1	0.25	9.045	0.0400	0.583
4	Orthorhombic No. 2	0.25	10.78	0.0290	4.56

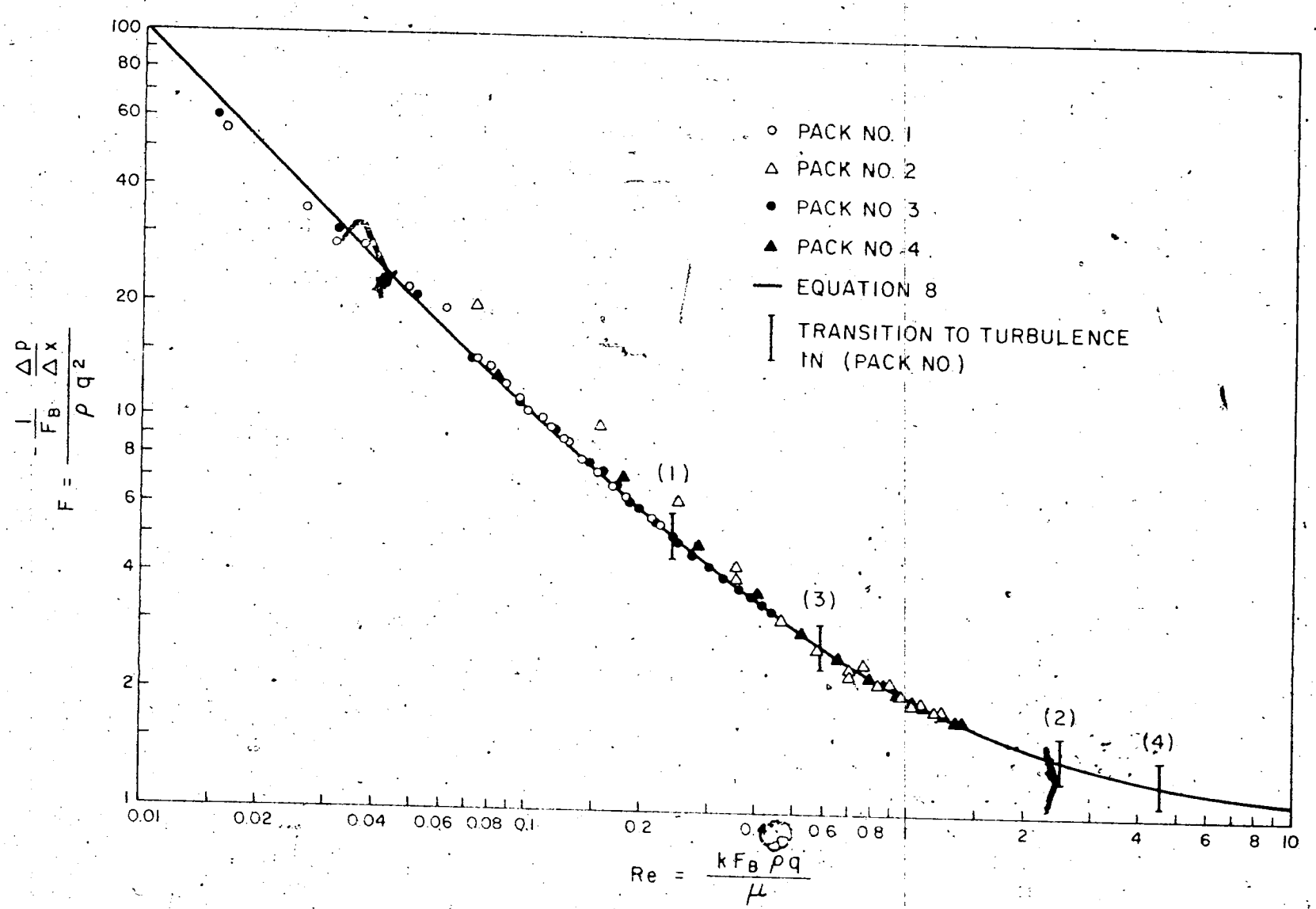

FIG. 16. FRICTION FACTOR, REYNOLDS NUMBER RELATIONSHIP FOR AQUEOUS GLYCERINE SOLUTION DATA

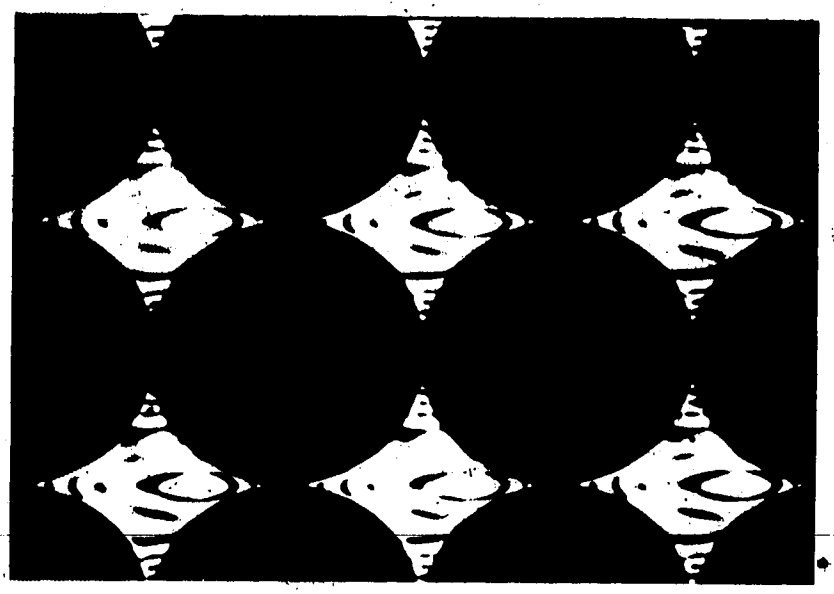

$R_e = 8.50 \times 10^{-2}$
LAMINAR FLOW

DIRECTION OF FLOW

$R_e = 3.18 \times 10^{-1}$
TURBULENT FLOW

PLATE 1. PHOTOGRAPHS OF ISOCHROMATIC PATTERNS IN PACK NO. 1 VISIBLE IN THE FLOWING MILLING YELLOW DYE SOLUTION.

DISCUSSION OF RESULTS

Bead Pack and Fluid Properties

The rheological data of the milling yellow dye solution, illustrated in Fig. 3, indicate that the solution behaves as a pseudo-plastic. Two of the three regions in its rheological behavior are apparent; firstly, a region of constant viscosity of about 0.28 poise at low shear rates, and secondly, a region of decreasing apparent viscosity at higher shear rates that appears as a straight line on this log-log plot. Data points at sufficiently high shear rates to define a second region of constant but smaller viscosity, were not obtained due to equipment limitations. Some scatter is apparent in the data due primarily to fluctuations of up to 1.0°C in the temperature of the sample during measurement on the Weissenberg rheogoniometer.

Figures 4 to 7 illustrate the pressure drop versus superficial velocity data obtained on the four packs using the aqueous glycerine solution. The data scatter appears to be small for all packs. The measurement of flowrates in the calibration of the rotameters indicated a reproducibility in the order of 1%. The errors in measurements of the head loss ranged up to 3.8% for the low velocity data on Pack No. 1.

Examination of the 95% confidence limits on the parameters k and F_B in Table 3 illustrates an important consideration in any future work of this nature. The uncertainties in the estimates of k for Packs No. 2 and No. 4 are up to six times larger than that for Packs No. 1 and No. 3. It is in Packs No. 2 and No. 4 that one should expect to obtain some data points within the Darcy flow region. Consequently, fitting a

quadratic equation, Eq. 3, to this region will result in a poor fit. If a smaller bead size, a tighter packing arrangement, or a more viscous solution is used in any future studies, all of which will increase the pressure drop and facilitate measurement at lower velocities, some type of data discrimination might be required in order to separate that region described by Darcy's law and that region described by Eq. 3. Because of the relatively large bead sizes, the loose packing arrangements and the low solution viscosity, very little strictly viscous data was obtained in this study. The uncertainty in the parameter estimates that can be attributed to using all of the data, including that at very low superficial velocities, is likely very small.

Tables A.1 to A.4 in the Appendix illustrate values of Re, calculated from Eq. 5, for the aqueous glycerine solution data that appears in Figs. 4 to 7. Once a value of Re at the transition to turbulence had been calculated from the milling yellow dye solution data, a check was made in order to ensure that the aqueous glycerine solution data used in estimating k and F_B did not exceed this value of Re. Since the applicability of Eq. 3 to the turbulent region has not been established, any turbulent data should not be included in estimating k and F_B. However, none of the aqueous glycerine solution data obtained in this study were found to be in the turbulent region.

Transition to Turbulence

As indicated in Figs. 8 to 11, scatter in the head loss versus mass flowrate data for the milling yellow dye solution is not large. However, the data were smoothed by eye and only a small number of points were selected for each pack from which a μ_e versus q curve was

established. Calibration of the rotameters indicated a reproducibility in the flowrate measurements within 1%. Errors in the head loss measurements dropped to a maximum of about 1%, as opposed to the much higher errors with the aqueous glycerine solution, as a result of the larger head losses associated with the more viscous solution. Data points were taken up to and beyond the transition to turbulence, having established this transition by means of the polariscope.

Curves of μ_e versus q in Figs. 12 to 15 illustrate some interesting behavior. Savins (62) has indicated that the shape of the apparent viscosity curve should be the same for data obtained in a viscometer and that derived from porous media experiments. Examination of the μ_e versus q curves in Figs. 12 to 15 indicates that their shape closely resembles that of the μ_a versus $\dot{\gamma}$ curve in Fig. 3, obtained from the Weissenberg rheogoniometer measurements. Although a constant viscosity at low superficial velocities was not obtained except for Pack No. 1, due to equipment limitations in measuring very small head losses, extrapolation of the trends indicates a range of constant viscosities from 0.18 to 0.25 poise, compared to the value of 0.28 poise obtained in the Weissenberg rheogoniometer. The larger value of the latter may be due, almost entirely, to poor temperature control resulting in a sample temperature up to 1°C less than the 30.3°C temperature in the bead pack experiments. As expected, a straight line region is evident in all four curves. Although not apparent in the Weissenberg rheogoniometer data, all four μ_e versus q curves showed a tendency to flatten out to a second but lower viscosity ranging from 0.029 to 0.066 poise, typical of pseudoplastic behavior.

However, unexpected results are apparent at high superficial velocities. Figures 12 to 15 illustrate, that although the tendency of the μ_e versus q curve is to flatten out at high superficial velocities, calculated effective viscosities change rapidly at this point. For Packs No. 1 and No. 3, values of μ_e first increase then decrease with increasing values of q. For Packs No. 2 and No. 4, values of μ_e decrease rapidly with increasing values of q. This unexpected behavior can be explained by examining the superficial velocities at the transition to turbulence, as determined by the visualization technique, indicated in Figs. 12 to 15. The change in the expected shape of the μ_e versus q curve, which closely corresponds to the onset of turbulence in each pack, can probably be attributed to the failure of Eq. 3 to adequately describe the pressure drop - flowrate relationship once turbulence appears. In turn, Eq. 9 probably does not adequately describe the μ_e versus q relationship once turbulence appears. Presumably some higher order equation might be required in this region.

Despite the limitations of these data at high superficial velocities, the values of μ_e at the transition to turbulence, as indicated in Table 4, are probably valid. In all but Pack No. 4, these values of μ_e are from an interpolated region of μ_e versus q behavior. The value of μ_e at the transition to turbulence in Pack No. 4 was determined from an extrapolation of the μ_e versus q curve into the region in which a constant effective viscosity is expected. This results in a value of μ_e at the transition to turbulence about 15% higher than that value from a curve through the measured points.

No difficulties were experienced in observing the onset of unsteady motion with the streaming birefringence visualization technique. The excellent visual quality of the interference patterns is apparent in Plate 1. The first unsteady motion of these patterns eventually develops into full scale turbulence at higher velocities, as illustrated in the bottom photograph of Plate 1. Of course the ease of viewing was superior in the 0.5 in. cubic pack. The void space in the 0.25 in. orthorhombic pack was near the limit of clear visualization, although higher magnification would facilitate observation of interference patterns in smaller voids. However, a noticeable degradation with time of the visual quality of the interference patterns took place. In this regard, the effective life of milling yellow dye solutions is probably in the order of nine months.

Turbulence commenced almost uniformly across the width of each pack at the observation point midway between the pressure taps. The flow diffuser proved to be effective in preventing channeling of the flow. Errors in the reproducibility of the superficial velocities at the transition to turbulence did not exceed 3.5%. As indicated in Table 4, the Reynolds numbers at the transition to turbulence show up to a twenty fold difference, from Re 0.241 for Pack No. 1 to Re 4.56 for Pack No. 4. It would appear then that based on a Reynolds number as defined by Eq. 5, the transition to turbulence does not take place at a single Re value or even over a very narrow range of Re values as was hoped for, but is a function of the bead size and packing arrangement. Alternately, one might conclude that the Reynolds number defined by Eq. 5 is not adequate. This behavior, in part, confirms the observation

made by Kingston and Nunge (63), that a change from a rhombohedral packing to a cubic packing has a great effect on the intensity of fully turbulent flow and may also have a large effect on the transition Reynolds number. Although the Reynolds number used in their studies, Re_D, incorporated the bead diameter as the length parameter, both representations of the Reynolds number, Re and Re_D, showed this sensitivity of the transition Reynolds number to geometry.

Table 5 is a comparison of values of Re_D at the transition to turbulence as determined in this study, with those determined by other authors. Values obtained in this study range from Re_D 123 for Pack No. 1 to Re_D 251 for Pack No. 4. Values determined by other authors range from Re_D 55 to Re_D 200, so that values obtained in this study are consistent with those in the literature. The value of Re_D at the transition to turbulence in Pack No. 4 exceeds the maximum value in the literature by 25%.

The question as to whether the use of $k F_B$ as the length parameter in the Reynolds number is an improvement over use of the bead diameter, remains unanswered. A single value or a very narrow range of values of the Reynolds number at the transition to turbulence has not been found using either $k F_B$ or D as the length parameter. The results from the aqueous glycerine solution flow studies, depicted in Fig. 16, encourage one to believe that a Reynolds number based on $k F_B$ as the length parameter, may be the route to follow. The data in Fig. 16 fortify the results of Ahmed and Sunada (64), suggesting that the friction factor F, versus Reynolds number Re, correlation represented by Eq. 8 may be a universal correlation for porous media and that data from all types of

TABLE 5. COMPARISON OF Re_D VALUES OF DIFFERENT AUTHORS AT THE TRANSITION TO TURBULENCE

AUTHOR	REFERENCE NO.	PACK DESCRIPTION	Re_D
Schneebeli	(1)	27 mm spheres and 1 in. gravel-random	60
Jolls and Hanratty	(15)	1 in. spheres-random	110-150
Chauveteau and Thirriot	(2)	two dimensional arbitrary shapes-random	80-180[a]
Wegner, Karabelas and Hanratty	(17)	3 in. spheres-cubic	90-120
Kyle and Perrine	(18)	two dimensional arrays of 0.5 in. cylinders - 3 porosities	55-13[b]
Kingston and Nunge	(19)	1.5 in. spheres-rhombohedral	80-200
This work		0.5 in. spheres-cubic	123
		0.5 in. spheres-orthorhombic	146
		0.25 in. spheres-cubic	153
		0.25 in. spheres-orthorhombic	251

a. based on hydraulic diameter
b. based on cylinder diameter

porous media will fall on a single curve when plotted in this manner. On the other hand, correlations of this kind based on a Reynolds number using the diameter D, as the length parameter, yield a variety of curves as shown by Fancher, Lewis and Barnes (65).

Certainly, additional data are required in order to examine further the specific effects of changes in flow geometry on the transition to turbulence in porous media. By continuing these studies with systematic sphere packs of varying diameters and packing arrangements, these effects can be more clearly defined.

A major requirement for the delineation of the transition to turbulence lies in any effort to establish an upper limit on the applicability of the Forchheimer equation. One can be fairly confident that the Forchheimer equation is adequate up to the end of laminar flow. Extension of flow studies into the turbulent region is necessary in order to determine whether or not a higher order equation is required. The definition of the range of a particular type of flow regime is an integral part of this process, particularly if a mechanistic model of the turbulent flow regime is to be developed.

CONCLUSIONS

As a result of this investigation, the following conclusions can be made:

1. Based on the Reynolds number Re, defined by Eq. 5, the transition to turbulence in a porous medium does not take place at a single value of Re, but in the case of ordered sphere packs, takes place at a value of Re that is a function of bead size and packing arrangement ranging from Re 0.241-4.56.

2. Although use of $k\,F_B$ as the length parameter in the Reynolds number Re, does not appear to improve the delineation of the transition to turbulence in terms of establishing a single value of Re, the results depicted in Fig. 16 suggest that this definition is a superior one, yielding an F versus Re correlation that appears to be universal.

3. The streaming birefringence visualization technique can be applied to qualitative studies of the flow regime character, and in particular to the transition to turbulence, in bead pack representations of natural porous media, thus eliminating the flow disturbance that results when intrusive techniques are employed.

4. Although other solutions might be used, solutions of milling yellow dye exhibit excellent birefringent qualities for visualization purposes.

5. The non-Newtonian nature of a birefringent solution can be analyzed, for purposes of defining a Reynolds number, by calculating an effective viscosity from that equation which describes the pressure drop - flowrate relationship in the particular flow regime of study. In this investigation, acceptable results were obtained by use of the Forchheimer equation to define an effective viscosity at the transition to turbulence.

6. Thin two-layer cubic and orthorhombic arrays can be used to determine the transition to turbulence in bead pack representations of natural porous media, with results comparable to those in much deeper packs, if the porosity effect at the pack wall is eliminated by use of half spheres at the wall.

RECOMMENDATIONS

The following recommendations are made:

1. Flow experiments in bead packs should be extended well above the transition to turbulence in order to investigate the applicability of the Forchheimer equation in this region. This requires that the parameters k and F_B first be determined in the laminar region, the limit of which is determined by identification of the transition to turbulence.

2. Higher heads and less viscous solutions can be used to extend these flow studies into the turbulent region.

3. Several additional packs, two layers in depth, should be constructed of varying bead size and packing arrangement, including an Orthorhombic No. 4 arrangement, to further investigate the transition to turbulence by means of the streaming birefringence visualization technique.

4. An attempt should be made to investigate the applicability of the streaming birefringence visualization technique to bead packs of depths greater than two layers.

5. If it is determined that a higher order equation is required in the turbulent region, this equation should be used in the calculation of the effective viscosities of the milling yellow dye solution in the turbulent region. This may result in the μ_e versus q curve flattening to a constant effective viscosity value corresponding to the value measured in a viscometer.

6. Some type of data discrimination should be used in determining the pack parameters k and F_B, in order to separate those data which are described by the Darcy equation and those which are described by the Forchheimer equation. This will improve the estimates of the pack parameters k and F_B.

7. Magnification of the image at the analyzer should be used to observe the isochromatic patterns in packs constructed of spheres having diameters less than 0.25 inches.

8. The use of the Forchheimer equation to calculate effective viscosities in this study, may have particular significance in the determination of a μ_e versus q curve for polymer solutions or other non-Newtonian solutions used as mobility control agents in waterflood schemes. The collapse of the μ_e versus q curve at high superficial velocities, observed in this study, suggests that the shape of this curve may be very sensitive to the flow equation used to calculate the effective viscosities. In the literature, invariably, development of a μ_e versus q curve from flow experiments with cores is accomplished by calculating effective viscosities from the Darcy equation. Anomalous increases in the effective viscosity at high velocities are explained by a variety of effects, from core plugging to the appearance of viscoelastic effects, although the latter effect is not observed in a viscometer. Unless one is reasonably sure that the flow is within the Darcy region, one might expect to obtain an increase in the effective viscosity at high velocities unless a higher order equation is

used. Thus the use of the Forchheimer equation in the interpretation of data of this kind should be investigated which, at the same time, would require the determination of the types of flow regimes that may exist over the range of data obtained.

NOMENCLATURE

A	bead pack cross-sectional area, cm^2
a	constant in Eq. 1
b	constant in Eq. 1
C_f	friction factor defined by Eq. 7, dimensionless
D	average sphere or particle diameter, cm
$f(\dot{\gamma})$	function of shear rate
F	friction factor, equal to $C_f/2$, dimensionless
F_A	viscous resistance coefficient, cm^{-2}
F_B	inertial resistance coefficient, cm^{-1}
H	head loss between upstream and downstream pressure taps, cm of flowing fluid
h_1	fluid level in upstream arm of manometer, cm
h_2	fluid level in downstream arm of manometer, cm
k	permeability, darcies
p	pressure, $dynes/cm^2$
q	superficial velocity, cm/sec
Re	Reynolds number defined by Eq. 5, dimensionless
Re_D	Reynolds number defined by Eq. 6, dimensionless
W	mass flowrate, gm/sec
X	distance between pressure taps, cm
x	horizontal distance along bead pack, cm
$\dot{\gamma}$	shear-rate, sec^{-1}
Δ	denotes finite difference

μ viscosity, poise

ρ density, gm/cm^3

Subscripts

a denotes an apparent value

e denotes an effective value

BIBLIOGRAPHY

(1) Schneebeli, G., "Experiments on the Range of Validity of Darcy's Law and the Appearance of Turbulence in a Filtering Flow", La Houille Blanche, No. 2, 141, (1955).

(2) Chauveteau, G., and Thirriot, Cl., "Régimes d'Ecoulement en Milieu Poreux et Limite de la Loi de Darcy", La Houille Blanche, No. 2, 141, (1967).

(3) Jones, W.M., "Viscous Drag and Secondary Flow in Granular Beds", Brit. J. Appl. Phys., Ser. 2, 1, 1559, (1968).

(4) Dudgeon, C.R., "An Experimental Study of the Flow of Water Through Coarse Granular Media", La Houille Blanche, No. 7, 785, (1968).

(5) Wright, D.E., "Nonlinear Flow Through Granular Media", J. Hydraulics Div. ASCE, 94, HY 4, 851, (1968).

(6) Scheidegger, A.E., "The Physics of Flow Through Porous Media", p. 127, University of Toronto Press, 1957.

(7) Ibid.

(8) Ghwyl, E., "An Analysis of Transient Gas Flow Through Porous Media", M.Sc. Thesis, Department of Chemical and Petroleum Engineering, University of Alberta, Edmonton, Alberta, 1968.

(9) Green, L., Jr., and Duwez, P., "Fluid Flow Through Porous Metals", Trans. ASME, J. App. Mech., 79, 39, (1951).

(10) Ibid.

(11) Fancher, G.H., Lewis, J.A., and Barnes, K., "Some Physical Characteristics of Oil Sands", Penn. State Coll. Mineral Ind. Exp. Sta., Bull. 12, 1933.

(12) Green, and Duwez, op cit.

(13) Ahmed, N., and Sunada, D.K., "Nonlinear Flow in Porous Media", J. Hydraulics Div. ASCE, 95, HY 6, 1847, (1969).

(14) Schneebeli, op. cit.

(15) Tolls, K.R., and Hanratty, T.J., "Transition to Turbulence for Flow Through a Dumped Bed of Spheres", Chem. Eng. Sci., 21, 1185, (1966).

(16) Chauveteau, and Thirriot, op. cit.

(17) Wegner, T.H., Karabelas, A.J., and Hanratty, T.J., "Visual Studies of Flow in a Regular Array of Spheres", Chem. Eng. Sci., 26, 59, (1971).

(18) Kyle, C.R., and Perrine, R.L., "An Experimental Model for Visual Studies of Turbulent Flow in Porous Materials", Can. J. Chem. Eng., 49, 19, (1971).

(19) Kingston, G., and Nunge, R.J., "Transition to Unsteady Flow and Intensity of Velocity Fluctuations in a Porous Medium", Can. J. Chem. Eng., 51, 246, (1973).

(20) Miller, E.B., "The Visualization of Turbulent Flows by Means of Flow Birefringence", Wyle Laboratories - Research Staff, Report WR 67-12, Huntsville, Alabama, July, 1967.

(21) Clayton, B.R., and Massey, B.S., "Flow Visualization in Water: A Review of Techniques", J. Sci. Instrum., 44, 2, (1967).

(22) Ibid.

(23) Hauser, E.A., and Dewey, D.R., "Visual Studies of Flow Patterns", J. Phys. Chem. 46, 212, (1942).

(24) Attinger, E.O., "Pulsatile Blood Flow", Chapter 9, p. 186, E.O. Attinger Ed., McGraw-Hill Book Co., New York, 1964.

(25) Miller, op. cit.

(26) Clayton, and Massey, op. cit.

(27) Frocht, M.M., "Photoelasticity", John Wiley & Sons, Inc., New York, Vol. I, 1941; Vol. II, 1948.

(28) Redner, S., "Photoelasticity", Vol. 9, p. 590-610, Encyclopedia of Polymer Science and Technology, John Wiley & Sons, Inc., New York, 1968.

(29) McPherson, M.B., and Nece, R.E., "An Inexpensive Demonstration Fluid Polariscope", Paper presented at the Spring Meeting of the Middle Atlantic Section of the American Society for Engineering Education, Lehigh University, Bethlehem, Pennsylvania, May, 1950.

(30) Prados, J.W., and Peebles, F.N., "Two-Dimensional Laminar Flow Analysis Utilizing a Doubly Refracting Liquid", A.I.Ch.E. Journal, 5, 225, (1959).

(31) Miller, op. cit.

(32) Peebles, F.N., Prados, J.W., and Honeycutt, E.H., Jr., "Birefringent and Rheologic Properties of Milling Yellow Suspensions", J. Polymer Science: Part C, No. 5, 37, (1964).

(33) Gogarty, W.B., "Rheological Properties of Pseudoplastic Fluids in Porous Media", Soc. Pet. Eng. J., 7, 149, (1967).

(34) Christopher, R.H., and Middleman, S., "Power-Law Flow Through a Packed Tube", I & EC Fundamentals, 4, 422, (1965).

(35) Sadowski, T.J., and Bird, R.B., "Non-Newtonian Flow Through Porous Media: I, Theoretical", Trans. Soc. Rheol., 9, 243, (1965).

(36) McKinley, R.M., Jahns, H.O., and Harris, W.W., "Non-Newtonian Flow in Porous Media", A.I.Ch.E. Journal, 12, 17, (1966).

(37) Gregory, D.R., and Griske, R.C., "Flow of Molten Polymers Through Porous Media", A.I.Ch.E. Journal, 13, 122, (1967).

(38) Burcik, E.J., "Pseudo Dilatant Flow of Polyacrylamide Solutions in Porous Media", Prod. Monthly, 31, 27, (1967).

(39) Burcik, E.J., and Perrer, J., "The Mechanism of Pseudo Dilatant Flow", Prod. Monthly, 32, 7, (1968).

(40) Dauben, D.L., and Menzie, D.L., "Flow of Polymer Solutions Through Porous Media", J. Pet. Tech., 19, 1065, (1967).

(41) Jennings, R.R., Rogers, J.H., and West, T.J., "Factors Influencing Mobility Control by Polymer Solutions", J. Pet. Tech., 23, 391, (1971).

(42) Smith, F.W., "The Behavior of Partially Hydrolyzed Polyacrylamide Solutions in Porous Media", J. Pet. Tech., 22, 148, (1970).

(43) Bondor, P.L., Hirasaki, G.J., and Tham, M.J., "Mathematical Simulation of Polymer Flooding in Complex Reservoirs", Soc. Pet. Eng. J., 12, 369, (1972).

(44) Savins, J.G., "Non-Newtonian Flow Through Porous Media", Ind. and Eng. Chem., 61, 18, (1969).

(45) Jennings, Rogers, and West, op. cit.

(46) Kyle, and Perrine, op. cit.

(47) Chauveteau, and Thirriot, op. cit.

(48) Graton, L.C., and Fraser, H.J., "Systematic Packing of Spheres", J. Geol., 43, 785, (1935).

(49) Kingston, and Nunge, op. cit.

(50) Dudgeon, C.R., "Wall Effects in Permeameters", J. Hydraulics Div. ASCE, 93, HY 5, 137, (1967).

(51) Martin, J.J., McCabe, W.L., and Monrad, C.C., "Pressure Drop Through Stacked Spheres", Chem. Eng. Progr., 47, 91, (1951).

(52) Mickley, H.S., Smith, K.A., and Korchak, E.I., "Fluid Flow in Packed Beds", Chem. Eng. Sci., 20, 237, (1965).

(53) Van der Merwe, D.F., and Gauvin, W.H., "Pressure Drag Measurements for Turbulent Air Flow Through a Packed Bed", A.I.Ch.E. Journal, 17, 402, (1971).

(54) Wegner, Karabelas, and Hanratty, op. cit.

(55) Gratton, and Fraser, op. cit.

(56) Mickley, Smith, and Korchak, op. cit.

(57) Van der Merwe, and Gauvin, op. cit.

(58) Ibid.

(59) Miller, op. cit.

(60) Ibid.

(61) Muraoka, D., "The Study of the Wake Behind a Suspended Oscillating Sphere in Vertical Laminar Flow Using a Solution of Birefringent Dye", Unpublished work, Dept. of Chemical Engineering, Montana State University, Bozeman, Montana, 1971.

(62) Savins, op. cit., p. 81.

(63) Kingston, and Nunge, op. cit.

(64) Ahmed, and Sunada, op. cit.

(65) Fancher, Lewis, and Barnes, op. cit.

APPENDIX

Sample Calculation

For the first aqueous glycerine solution data point obtained on Pack No. 1, the following calculation procedure yields the processed data $\Delta p/\Delta x$ and q, in Table A:1:

For

$$H = 0.130 \text{ cm}$$

$$W = 5.250 \frac{\text{gm}}{\text{sec}}$$

Then

$$\frac{\Delta p}{\Delta x} = \frac{H \rho g}{X}$$

$$= \frac{(0.130)(1.1877)(980.66)}{20.384}$$

$$= 7.428 \frac{\text{dynes}}{\text{cm}^2} \frac{1}{\text{cm}}$$

$$q = \frac{W}{\rho A}$$

$$= \frac{5.250}{(1.1877)(16.419)}$$

$$= 0.26[illegible]2 \frac{\text{cm}}{\text{sec}}$$

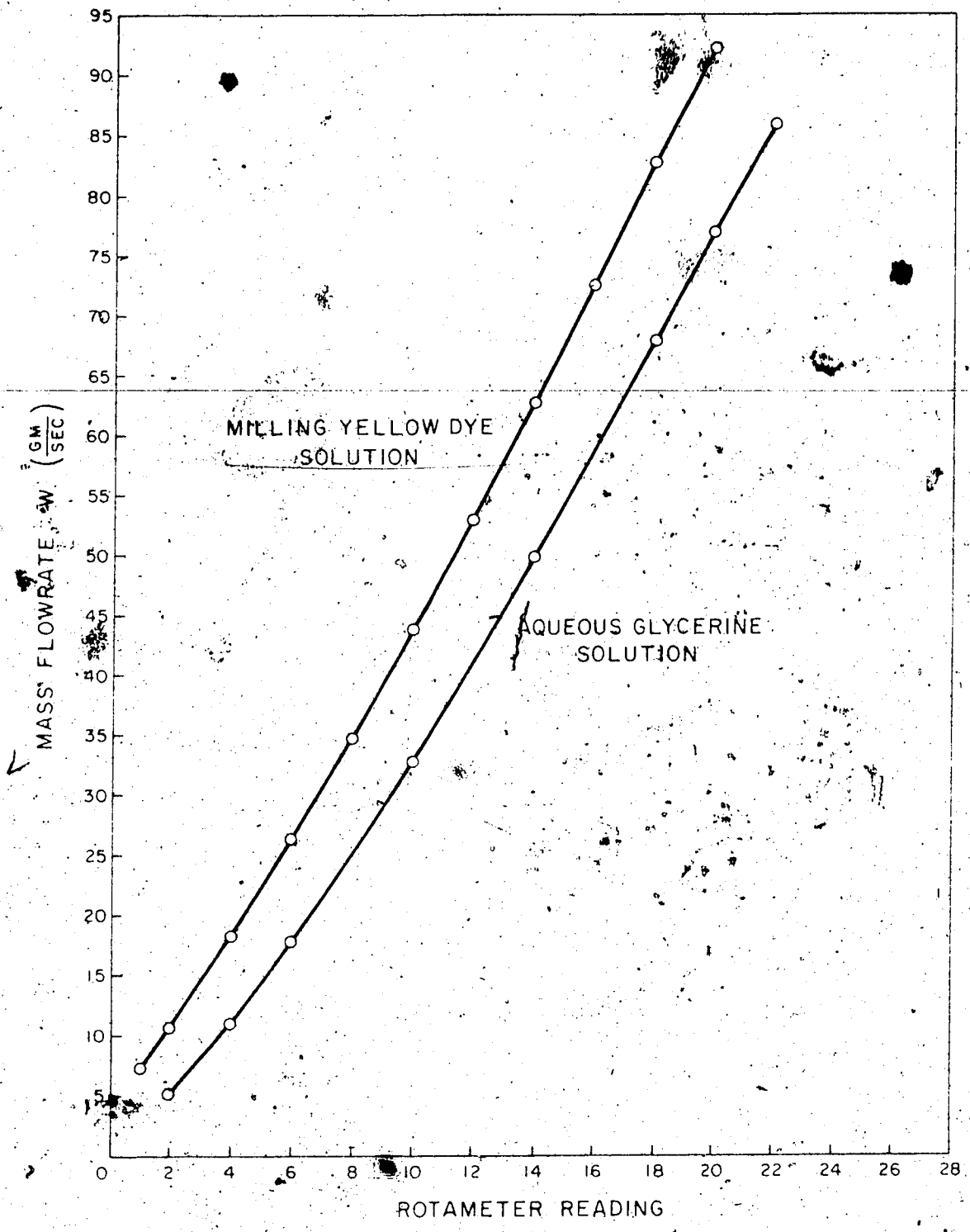

FIG. A.1. CALIBRATION CURVE FOR LOW RANGE ROTAMETER A.

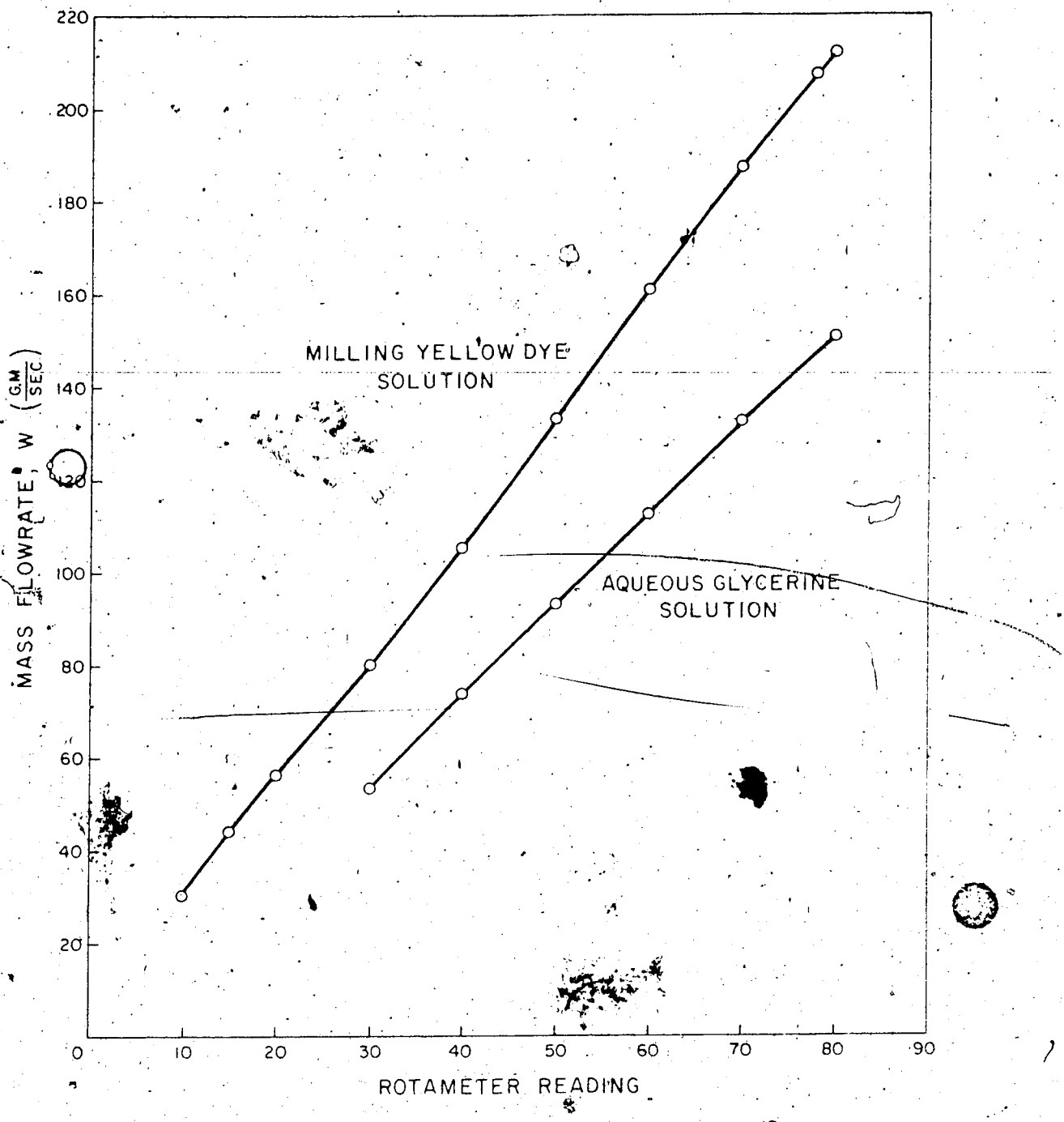

FIG. A.2. CALIBRATION CURVE FOR HIGH RANGE ROTAMETER B.

TABLE A.1 EXPERIMENTAL AND PROCESSED AQUEOUS GLYCERINE SOLUTION DATA FOR PACK NO. 1

h_1 (CM)	h_2 (CM)	ROTAMETER READING	H (CM)	W $(\frac{GM}{SEC})$	$\frac{\Delta p}{\Delta x}$ $(\frac{DYNES}{CM^2}\frac{1}{CM})$	q $(\frac{CM}{SEC})$	Re	F
18.550	18.420	2 A	0.130	5.250	7.428	0.2692	7.81×10^{-3}	122.
18.810	18.545	4 A	0.265	11.05	15.14	0.5666	1.64×10^{-2}	56.1
18.940	18.515	6 A	0.425	17.65	24.28	0.9051	2.63×10^{-2}	35.3
19.235	18.735	7 A	0.500	21.20	28.57	1.087	3.15×10^{-2}	28.8
19.330	18.640	8 A	0.690	25.00	39.43	1.282	3.72×10^{-2}	28.6
19.685	18.765	10 A	0.920	32.80	52.57	1.682	4.88×10^{-2}	22.1
20.110	18.950	12 A	1.160	41.05	66.28	2.105	6.11×10^{-2}	19.4
20.670	19.260	14 A	1.410	49.75	80.57	2.551	7.40×10^{-2}	14.7
25.835	24.255	30 B	1.580	54.00	90.28	2.769	8.03×10^{-2}	14.0
21.195	19.500	16 A	1.695	58.80	96.85	3.015	8.75×10^{-2}	12.7
26.135	24.290	35 B	1.845	63.80	105.4	3.277	9.51×10^{-2}	11.7
21.660	19.760	18 A	1.900	67.80	108.6	3.477	1.01×10^{-1}	10.7
26.890	24.750	40 B	2.140	73.80	122.3	3.784	1.10×10^{-1}	10.2
22.455	20.240	20 A	2.215	76.80	126.6	3.938	1.14×10^{-1}	9.71
27.630	25.195	45 B	2.435	83.40	139.1	4.277	1.12×10^{-1}	9.06
23.250	20.700	22 A	2.550	85.85	145.7	4.402	1.28×10^{-1}	8.95
28.145	25.440	50 B	2.705	93.20	154.6	4.779	1.39×10^{-1}	8.06
30.175	27.125	55 B	3.050	103.1	174.3	5.287	1.53×10^{-1}	7.42
31.030	27.640	60 B	3.390	112.9	193.7	5.789	1.68×10^{-1}	6.88
31.760	27.975	65 B	3.785	122.8	216.3	6.297	1.83×10^{-1}	6.49
33.105	29.015	70 B	4.090	132.4	233.7	6.789	1.97×10^{-1}	6.04
31.870	27.410	75 B	4.460	141.9	254.8	7.277	2.11×10^{-1}	5.73
32.810	27.950	80 B	4.860	151.0	277.7	7.743	2.25×10^{-1}	5.51

TABLE A.2 EXPERIMENTAL AND PROCESSED AQUEOUS GLYCERINE SOLUTION DATA FOR PACK NO. 2

h_1 (CM)	h_2 (CM)	ROTAMETER READING	H (CM)	W ($\frac{CM}{SEC}$)	$\frac{\Delta P}{\Delta x}$ ($\frac{DYNES}{CM^2} \frac{1}{CM}$)	q ($\frac{CM}{SEC}$)	Re	F
28.805	28.670	2 A	0.215	5.250	13.93	0.2939	7.39×10^{-2}	20.1
29.135	28.670	4 A	0.465	11.05	30.14	0.6186	1.55×10^{-1}	9.83
29.135	28.370	6 A	0.765	17.65	49.58	0.9880	2.48×10^{-1}	6.34
29.350	28.370	8 A	0.980	25.00	63.52	1.399	3.52×10^{-1}	4.05
29.350	28.310	8 A	1.040	25.00	67.40	1.399	3.52×10^{-1}	4.30
29.610	28.310	10 A	1.300	32.80	84.26	1.836	4.61×10^{-1}	3.12
29.805	28.065	12 A	1.740	41.05	112.8	2.298	5.78×10^{-1}	2.67
30.550	28.370	14 A	2.180	49.75	141.3	2.785	7.00×10^{-1}	2.27
30.620	28.370	14 A	2.250	49.75	145.8	2.785	7.00×10^{-1}	2.35
20.405	17.675	30 B	2.730	54.[illegible]	176.9	3.023	7.60×10^{-1}	2.42
32.225	29.350	16 A	2.875	58.80	186.3	3.292	8.27×10^{-1}	2.15
32.225	29.400	16 A	2.825	58.80	183.1	3.292	8.27×10^{-1}	2.11
21.285	17.810	35 B	3.475	63.90	225.2	3.577	8.99×10^{-1}	2.20
33.015	29.400	18 A	3.615	67.85	234.3	3.795	9.54×10^{-1}	2.03
21.890	17.810	40 B	4.080	73.80	264.4	4.131	1.04×10^{0}	1.93
33.995	29.565	20 A	4.430	76.80	287.1	4.299	1.08×10^{0}	1.94
23.470	18.465	45 B	5.005	83.40	324.4	4.669	1.17×10^{0}	1.86
34.860	29.565	22 A	5.295	85.85	343.2	4.806	1.21×10^{0}	1.85

TABLE A.3 EXPERIMENTAL AND PROCESSED AQUEOUS GLYCERINE SOLUTION DATA FOR PACK NO. 3

h_1 (CM)	h_2 (CM)	ROTAMETER READING	H (CM)	W ($\frac{GM}{SEC}$)	$\frac{\Delta p}{\Delta x}$ ($\frac{DYNES}{CM^2} \cdot \frac{1}{CM}$)	q ($\frac{CM}{SEC}$)	Re	F
35.315	34.410	2 A	0.905	5.250	52.36	0.5379	1.52×10^{-2}	60.2
36.300	34.230	4 A	2.070	11.05	119.8	1.132	3.21×10^{-2}	31.1
37.825	34.230	6 A	3.595	17.65	208.0	1.808	5.12×10^{-2}	21.1
38.865	33.835	8 A	5.030	25.00	291.0	2.561	7.25×10^{-2}	14.7
40.550	33.835	10 A	6.715	32.80	388.5	3.360	9.52×10^{-2}	11.4
42.065	33.280	12 A	8.785	41.05	508.3	4.206	1.19×10^{-1}	9.55
43.540	32.855	14 A	10.685	49.75	618.2	5.097	1.44×10^{-1}	7.91
51.580	39.710	30 B	11.870	54.00	686.8	5.532	1.57×10^{-1}	7.46
45.335	32.310	16 A	13.025	58.80	753.6	6.024	1.71×10^{-1}	6.90
53.385	39.170	35 B	14.215	63.90	822.5	6.547	1.85×10^{-1}	6.38
47.090	31.725	18 A	15.365	67.80	889.0	6.946	1.97×10^{-1}	6.12
55.340	38.485	40 B	16.855	73.80	975.	7.561	2.14×10^{-1}	5.67
48.965	31.100	20 A	17.865	76.80	1034.	7.868	2.23×10^{-1}	5.55
57.290	37.880	45 B	19.410	83.40	1123.	8.545	2.42×10^{-1}	5.14
51.025	30.565	22 A	20.460	85.85	1184.	8.796	2.49×10^{-1}	5.09
59.405	37.480	50 B	21.925	93.20	1269.	9.549	2.70×10^{-1}	4.62
61.700	36.725	55 B	24.975	103.1	1445.	10.56	2.99×10^{-1}	4.31
64.200	36.175	60 B	28.025	112.9	1622.	11.57	3.28×10^{-1}	4.03
66.685	35.480	65 B	31.205	122.8	1806.	12.58	3.56×10^{-1}	3.79
69.170	34.790	70 B	34.380	132.4	1989.	13.56	3.84×10^{-1}	3.59
71.600	33.970	75 B	37.630	141.9	2177.	14.54	4.12×10^{-1}	3.42
74.220	33.045	80 B	41.175	151.0	2382.	15.47	4.38×10^{-1}	3.31

TABLE A.4 EXPERIMENTAL AND PROCESSED AQUEOUS GLYCERINE SOLUTION DATA FOR PACK NO. 4

h_1 (CM)	h_2 (CM)	ROTAMETER READING	H (CM)	W $(\frac{GM}{SEC})$	$\frac{\Delta p}{\Delta x}$ $(\frac{DYNES}{GM^2}\frac{1}{CM})$	q $(\frac{CM}{SEC})$	Re	F
41.210	39.835	2 A	1.375	5.250	79.56	0.6211	8.36×10^{-2}	13.0
42.625	39.305	4 A	3.320	11.05	192.1	1.307	1.76×10^{-1}	6.68
44.455	38.640	6 A	5.815	17.65	336.5	2.038	2.81×10^{-1}	4.56
43.355	37.685	8 A	8.670	25.00	501.6	2.958	3.98×10^{-1}	3.51
48.715	36.805	10 A	11.910	32.80	689.1	3.880	5.23×10^{-1}	2.91
51.490	35.500	12 A	15.990	41.05	925.2	4.856	6.54×10^{-1}	2.53
54.915	33.785	14 A	21.130	49.75	1223.	5.886	7.93×10^{-1}	2.26
62.350	38.260	30 B	24.090	54.00	1394.	6.388	8.60×10^{-1}	2.16
58.485	31.875	16 A	26.610	58.80	1540.	6.956	9.37×10^{-1}	2.07
67.060	36.635	35 B	30.425	63.90	1760.	7.560	1.02×10^{0}	1.98
62.945	29.700	18 A	33.245	67.80	1924.	8.021	1.08×10^{0}	1.93
71.880	34.085	40 B	37.795	73.80	2187.	8.731	1.18×10^{0}	1.85
67.420	27.000	20 A	40.420	76.80	2339.	9.086	1.22×10^{0}	1.82
77.250	31.005	45 B	46.245	83.40	2676.	9.866	1.33×10^{0}	1.75
73.305	24.550	22 A	48.755	85.85	2821.	10.16	1.37×10^{0}	1.73

TABLE A.5 EXPERIMENTAL AND PROCESSED MILLING YELLOW DYE SOLUTION H vs W DATA FOR PACK NO. 1

h_1 (CM)	h_2 (CM)	ROTAMETER READING	H (CM)	W $(\frac{GM}{SEC})$
39.330	38.910	1 A	0.420	7.450
39.435	38.810	2 A	0.625	10.70
39.605	38.810	3 A	0.795	14.50
39.605	38.660	4 A	0.945	18.40
40.035	38.985	5 A	1.050	22.30
39.850	38.830	6 A	1.020	26.45
39.975	38.830	7 A	1.145	30.55
41.795	40.665	10 B	1.140	31.00
39.975	38.745	8 A	1.230	34.95
40.000	38.740	9 A	1.260	39.10
40.415	39.005	10 A	1.410	43.60
40.405	38.865	12 A	1.540	52.50
42.545	40.805	20 B	1.740	56.00
40.750	39.005	14 A	1.745	62.50
42.690	40.710	25 B	1.980	68.90
41.330	39.315	16 A	2.015	72.50
42.990	40.845	30 B	2.145	81.50
41.610	39.415	18 A	2.195	82.65
41.875	39.460	20 A	2.415	92.35
43.330	40.845	35 B	2.485	94.10
44.075	41.265	40 B	2.810	106.9
44.510	41.215	45 B	3.295	120.0
45.195	41.370	50 B	3.825	133.8
46.290	41.705	55 B	4.585	147.9
47.115	41.780	60 B	5.335	161.0
48.165	42.110	65 B	6.055	174.3
48.660	41.965	70 B	6.695	187.0

TABLE A.6 EXPERIMENTAL AND PROCESSED MIELING YELLOW DYE SOLUTION

H vs W DATA FOR PACK NO. 2

h_f (CM)	h_o (CM)	ROTAMETER READING	H (CM)	W $\left(\frac{CM}{SEC}\right)$
41.355	40.860	2 A	0.295	10.70
41.860	40.840	4	1.020	18.40
42.135	40.840	6 A	1.295	26.45
42.135	40.600	8 A	1.535	34.95
42.465	40.600	10 A	1.865	43.60
43.070	40.790	12 A	2.280	52.50
66.700	64.360	20 B	2.340	56.00
43.890	41.070	14 A	2.820	62.50
67.575	64.405	25 B	3.170	68.90
44.195	40.545	16 A	3.650	72.50
68.425	64.200	30 B	4.225	81.50
45.115	40.625	18 A	4.490	82.65
46.420	40.890	20 A	5.530	92.35
69.380	64.060	35 B	5.320	94.10
70.535	63.945	40 B	6.590	106.9
71.700	63.750	45 B	7.950	120.0
73.290	63.860	50 B	9.430	133.8
75.050	64.090	55 B	10.960	147.7
76.385	63.820	60 B	12.565	161.0
78.320	64.020	65 B	14.300	174.3
79.985	63.910	70 B	16.075	187.0

TABLE A.7 EXPERIMENTAL AND PROCESSED MILLING YELLOW DYE SOLUTION

H vs W DATA FOR PACK NO. 3.

h_1 (CM)	h_2 (CM)	DIAMETER READING	H (CM)	W $(\frac{GM}{SEC})$
44.575	42.260	1 A	2.315	7.450
44.975	42.120	2 A	2.855	10.70
45.475	42.035	3 A	3.440	14.50
45.400	41.665	4 A	3.735	18.40
45.775	41.480	5 A	4.295	22.30
46.240	41.480	6 A	4.760	26.45
46.510	41.230	7 A	5.280	30.55
47.400	41.730	8 A	4.670	34.95
47.790	41.650	9 A	6.140	39.10
48.130	41.370	10 A	6.760	43.60
48.805	41.320	12 A	7.485	52.50
47.050	38.865	20 B	8.185	56.00
49.680	41.060	14 A	8.620	62.50
48.110	38.385	25 B	9.725	68.90
51.150	40.890	16 A	10.260	72.50
50.080	38.165	30 B	11.915	81.50
52.010	39.715	18 A	12.295	84.65
54.180	39.250	20 A	14.930	92.35
51.620	36.800	35 B	14.820	94.10
54.485	35.875	40 B	18.610	106.9
56.680	34.925	4	21.755	120.0
59.600	33.700	50 B	25.900	133.8
62.310	32.060	55 B	30.250	147.7
65.475	31.060	60 B	34.415	161.0
68.170	29.220	65 B	38.950	174.3
71.450	28.065	70 B	43.385	187.0

TABLE A.8 EXPERIMENTAL AND PROCESSED MILLING YELLOW DYE SOLUTION

H vs. W DATA FOR PACK NO. 4

h_1 (CM)	h_2 (CM)	ROTAMETER READING	H (CM)	W ($\frac{GM}{SEC}$)
59.760	56.355	1 A	3.405	7.450
60.565	56.355	2 A	4.210	10.70
61.055	55.940	3 A	5.110	14.50
61.735	55.940	4 A	5.795	18.40
62.095	55.550	5 A	6.545	22.30
62.970	55.550	6 A	7.420	26.45
63.520	54.845	7 A	8.675	30.55
64.710	54.845	8 A	9.865	34.95
65.530	54.315	9 A	11.215	39.10
66.860	53.725	10 A	13.135	43.60
69.940	51.955	12 A	17.985	52.50
85.715	65.575	20 B	20.140	56.00
74.970	49.920	14 A	24.050	62.50
90.900	63.010	25 B	27.890	68.90
78.545	47.400	16 A	31.145	72.50
96.040	60.340	30 B	35.700	81.50
83.230	45.135	18 A	38.095	82.65
87.475	42.680	20 A	44.795	92.35
60.165	17.380	35 B	42.785	94.10
66.505	13.270	40 B	53.235	106.9
73.645	9.960	45 B	63.685	120.0
80.970	5.840	50 B	75.130	133.8
90.685	0.850	55 B	89.835	147.7

TABLE A.9 MILLING YELLOW DYE SOLUTION EFFECTIVE VISCOSITIES CALCULATED FROM EQ. 9, USING SMOOTHED H vs W DATA FOR PACK NO. 1

H (CM)	v (CM/SEC)	$\frac{dp}{dx}$ (DYNES/CM³)	q (CM/SEC)	μ_e (POISE)
0.420	7.450	21.47	0.4269	1.757×10^{-1}
0.620	10.70	31.70	0.6132	1.801×10^{-1}
0.800	14.60	40.90	0.8310	1.709×10^{-1}
0.960	20.00	49.08	1.146	1.475×10^{-1}
1.160	30.00	59.31	1.719	1.167×10^{-1}
1.350	40.00	69.02	2.293	9.96×10^{-2}
1.540	50.00	78.7	2.865	8.9×10^{-2}
1.735	60.00	88.71	3.438	8.161×10^{-2}
2.040	75.00	104.3	4.298	7.396×10^{-2}
2.390	90.00	122.2	5.158	6.966×10^{-2}
2.800	105.0	143.2	6.017	6.774×10^{-2}
3.300	120.0	168.7	6.877	6.808×10^{-2}
3.910	135.0	199.9	7.737	7.040×10^{-2}
4.680	150.0	239.3	8.596	7.514×10^{-2}
5.530	165.0	282.7	9.456	8.013×10^{-2}
6.330	180.0	323.6	10.32	8.304×10^{-2}

TABLE A.10 MILLING YELLOW DYE SOLUTION EFFECTIVE VISCOSITIES CALCULATED FROM EQ. 9, USING SMOOTHED H vs W DATA FOR PACK NO. 2

H (CM)	W $(\frac{CM}{SEC})$	$\frac{\Delta p}{\Delta x}$ $(\frac{DYNES}{CM^2} \frac{1}{CM})$	q $(\frac{CM}{SEC})$	η_e (POISE)
0.960	16.00	55.67	1.001	1.547×10^{-1}
1.230	25.00	91.33	1.564	1.099×10^{-1}
1.550	35.00	139.9	2.190	8.098×10^{-2}
2.130	50.00	123.5	3.128	5.451×10^{-2}
2.920	65.00	169.3	4.066	3.990×10^{-2}
4.080	80.00	236.6	5.005	3.641×10^{-2}
6.000	100.0	348.0	6.256	3.441×10^{-2}
7.950	120.0	461.1	7.507	2.427×10^{-2}
10.15	140.0	588.6	8.758	1.412×10^{-2}
12.53	160.0	726.7	10.01	2.687×10^{-3}
15.09	180.0	875.1	11.26	9.614×10^{-3}

TABLE A.11 MILLING YELLOW DYE SOLUTION EFFECTIVE VISCOSITIES CALCULATED FROM EQ. 9, USING SMOOTHED H vs W DATA FOR PACK NO. 3

H (CM)	W $(\frac{GM}{SEC})$	$\frac{dP}{dq}$ $(\frac{DYNES}{CM^2} \frac{1}{CM})$	q $(\frac{CM}{SEC})$	μ_e (POISE)
2.700	10.00	139.8	1.145	1.141×10^{-1}
3.520	15.00	182.2	1.717	9.725×10^{-2}
4.040	20.00	209.3	2.290	8.164×10^{-2}
5.120	30.00	265.1	3.435	6.511×10^{-2}
6.250	40.00	323.6	4.580	5.591×10^{-2}
7.320	50.00	[illegible]	5.725	4.868×10^{-2}
8.480	[illegible]	439.0	6.870	4.353×10^{-2}
10.70	75.00	554.0	8.587	3.968×10^{-2}
13.80	90.00	714.5	10.30	3.987×10^{-2}
17.60	105.0	911.2	12.02	4.163×10^{-2}
21.70	120.0	1124.	13.74	4.293×10^{-2}
30.92	150.0	1601.	17.17	4.503×10^{-2}
40.70	180.0	2107.	20.61	4.483×10^{-2}

TABLE A.12 MILLING YELLOW DYE SOLUTION EFFECTIVE VISCOSITIES CALCULATED FROM EQ. 9, USING SMOOTHED H vs W DATA FOR PACK NO. 4

H (CM)	W $(\frac{CM}{SEC})$	$\frac{\Delta p}{L}$ $(\frac{DYNES}{CM^2} \frac{1}{CM})$	q $(\frac{CM}{SEC})$	μ_e (POISE)
3.300	7.500	170.9	0.9916	1.390×10^{-1}
5.100	15.00	264.0	1.983	9.244×10^{-2}
6.150	20.00	318.4	2.644	7.317×10^{-2}
8.500	30.00	440.1	3.966	4.86×10^{-2}
11.80	40.00	610.9	5.288	3.64×10^{-2}
22.30	60.00	1155.	7.933	3.032×10^{-2}
35.60	80.00	1843.	10.58	2.307×10^{-2}
49.00	100.0	2537.	13.22	6.083×10^{-3}
64.00	120.0	3314.	15.87	-1.148×10^{-2}
81.80	140.0	4235.	18.51	-2.642×10^{-2}